Contract No:

This document was prepared in conjunction with work accomplished under Contract No. 89303321CEM000080 with the U.S. Department of Energy (DOE) Office of Environmental Management (EM).

Additive Manufacturing Flaw Assessment Methodology

Final Report

To

Savanah River National Lab

(Contract No. 00005000456)

By

Welded Structures Lab
Department of Naval Architecture and Marine Engineering
University of Michigan
Contact: dongp@umich.edu

September 2022

Contents

1. INTRODUCTION

An evolution fatigue data and flaw tolerance of components produced using the Powder Bed Fusion (PBF) Additive Manufacturing (AM) process is documented in this report. Initial differences in fatigue data for AM components compared to smooth bar fatigue data indicated a need for a more detailed analysis of AM data available in technical literature. The investigation was initiated to support the development of a fatigue analysis methodology for AM components to support the of codification of AM technology for pressure equipment.

The project was initiated to collect and analyze stainless steel 304L and 316L AM fatigue test data and corresponding process and quality information to develop S-N and E-N based fatigue data representation. Additional AM fatigue test data including Inconel Ti-6-4 and aluminum alloys were also considered for comparison purposes

Metallic AM parts tend to contain various forms of defects distributed throughout the part, as shown in Figure 1-1[1, 2]. If an AM part is subjected to fatigue loading in service, a fatigue analysis needs to be performed during the design process to ensure an acceptable service life for the part. Post-process machining and polishing do not to improve fatigue resistance in any significant degree. The low cycle fatigue regime is of particular interest to this project in support of flaw acceptance criteria currently under development by ASME's BPTCS/BNCS. Internal defects become exposed as external surface defects, as illustrated in Figure 1-2 [3] during machining for the machining of the AM part to final dimensions. This implies that as long as inherent AM defects are within a controlled limit in terms of both size and distribution characteristics (see Figure 1-3 [1]), the corresponding fatigue test data in terms of either S-N (stress life) or E-N (strain life) can be investigated and characterized to establish fatigue properties of AM parts for design and fatigue evaluation purposes. The resulting S-N or E-N curves and their scatter bands can be used to derive fatigue design allowable stress values by capturing the effects of distributed discontinuities within an acceptable limit.

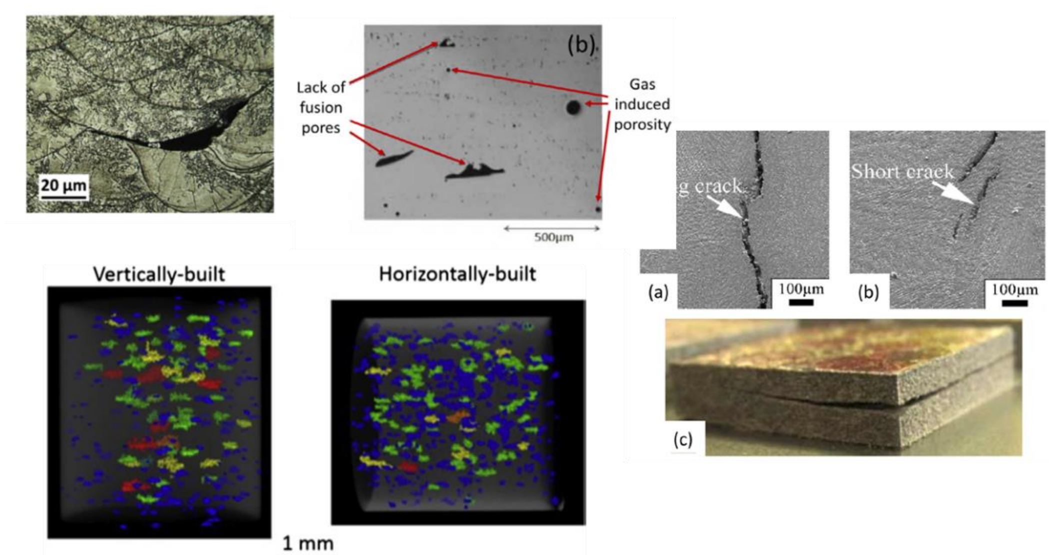

Figure 1-1

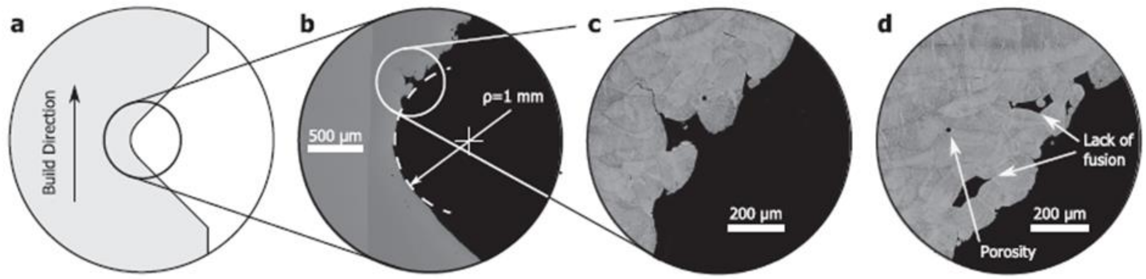

Figure 1-2

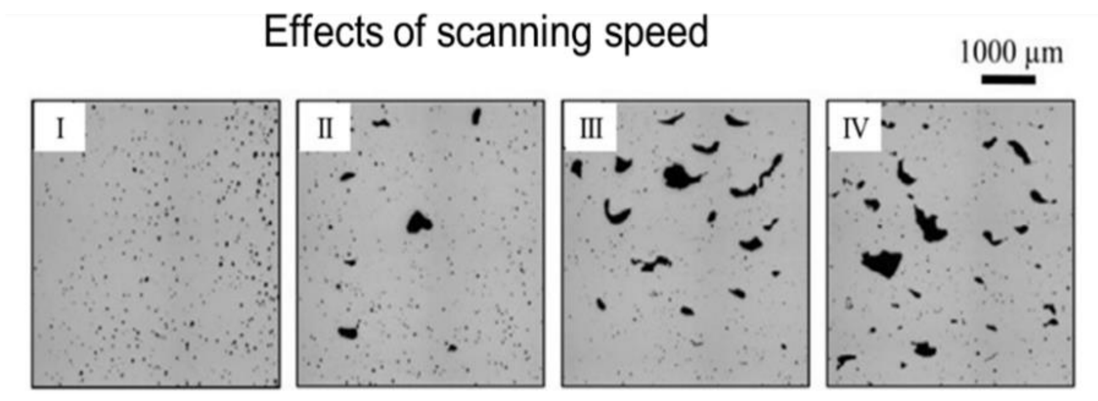

(I) 250 (II) 500 (III) 750 and (IV) 1000 mm/s

Figure 1-3

2. TECHNICAL DEVELOPMENTS

2.1 Evaluation and Characterization of AM Defects

It has been well established that fatigue properties are sensitive to defects or geometric discontinuities. The project started with a comprehensive assessment of literature and reports with the focus on the effects of AM defects on fatigue performance for Stainless Steel 316L, and 304L. The assessment also included a detailed evaluation of any beneficial effects of post-process treatment, (e.g., stress relief, annealing, and hot isostatic pressing or HIP). The key findings are documented in this section.

2.1.1 Major AM Defect Types

A micrograph produced by Brenna et al [4] serves a good illustration of major defect types involved in directed-energy-deposition processed 17-4PH stainless steel, as show in **Error! Reference source not found.** which contains surface connected porosity, lack of fusion, and gas-entrapped pores. All these defects can serve as fatigue crack initiation sites and are of interest in this project.

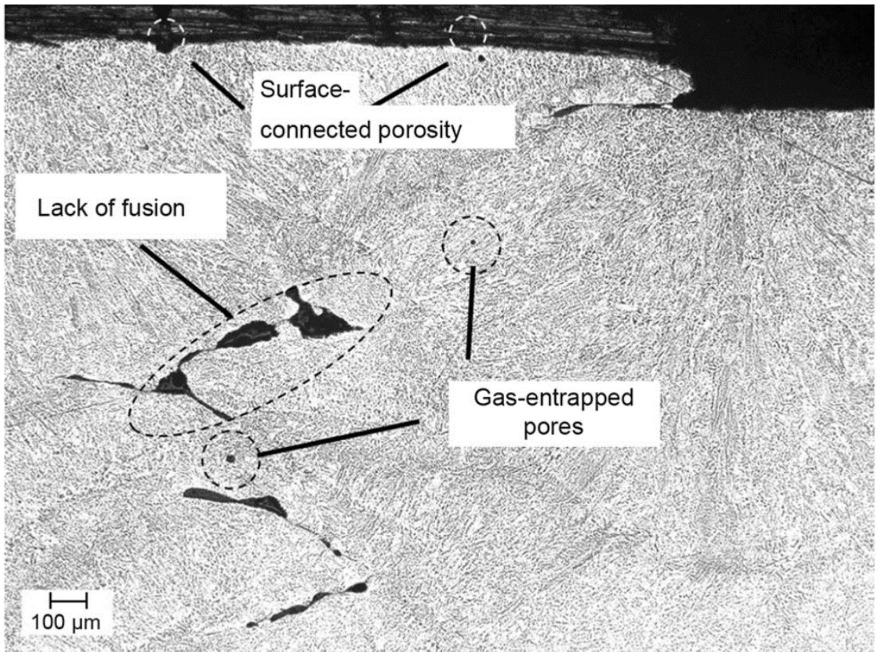

Figure 2-1

Lack of Fusion

The lack of fusion type of defects associated with PBF process can be mostly attributed to un-melted powder resulted from the use of excessive hatch spacing as illustrated in Figure 2-2 [5]. These lack of fusion defects (Figure 2-1and Figure 2-2) are most often in planar forms because of the layer-by-layer powder build strategy inherent in the PBF process.

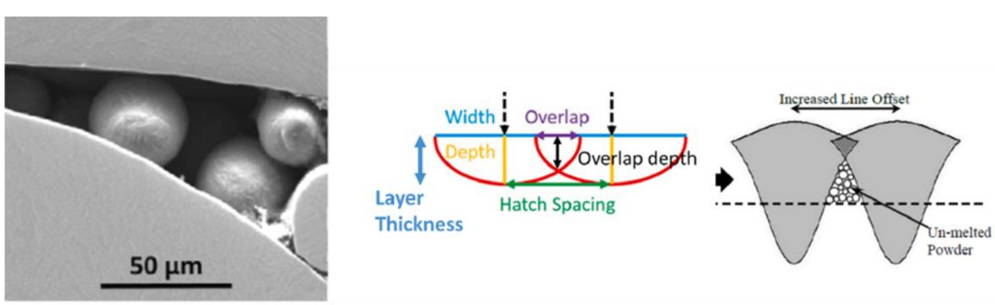

Figure 2-2

Gas Porosities

Gas-entrapped pores characterized by their spherical shapes, as shown in Figure 2-3 [6] from AM stainless steel samples. Figure 2-3a and Figure 2-3b show the effects of powder layer thickness effects on the level of porosities, at 60 μm and 150 μm, respectively. Figure 2-3c shows a cross-section micrograph view of a sample cross-section corresponding to the conditions shown in Figure 2-3a. Although solidification cracking or hot cracking have been often documented for other metal types, it has not been seen in stainless steel AM parts, at least for 316L. This is mainly due to its high ductility.

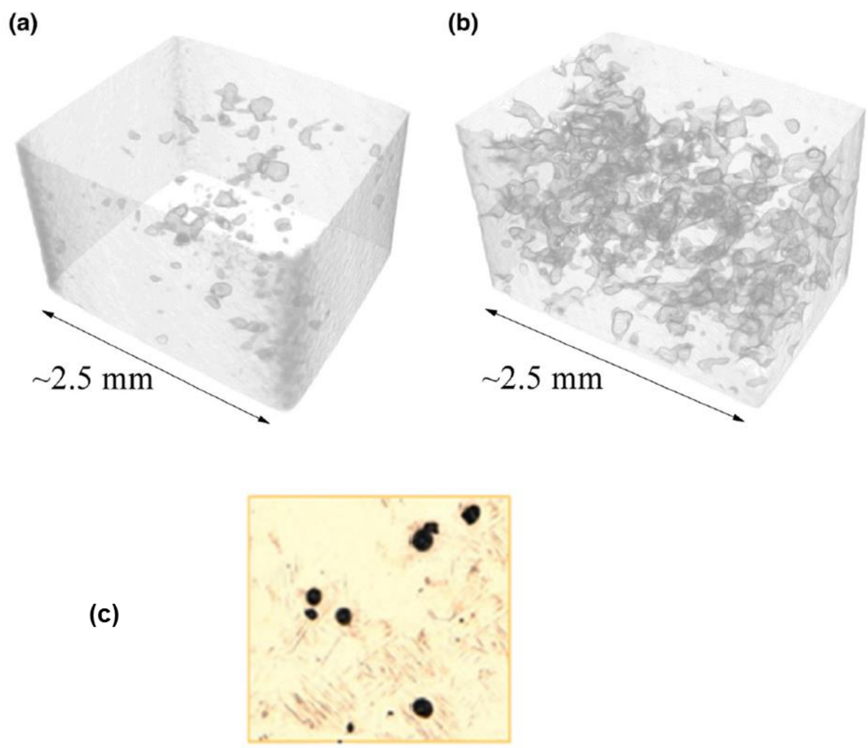

Figure 2-3

Surface Roughness and Defects

Inherent surface defects such as roughness accompanied by reentrant sharp corners or notches, as illustrated in Figure 2-4 with a cross-section view given in Figure 2-4a and a surface view (SEM) in Figure 2-4b, as well as a synchrotron radiation micro-tomography view [7]. These surface features can be significantly more detrimental to fatigue than internal defects, as to be further discussed in later sections.

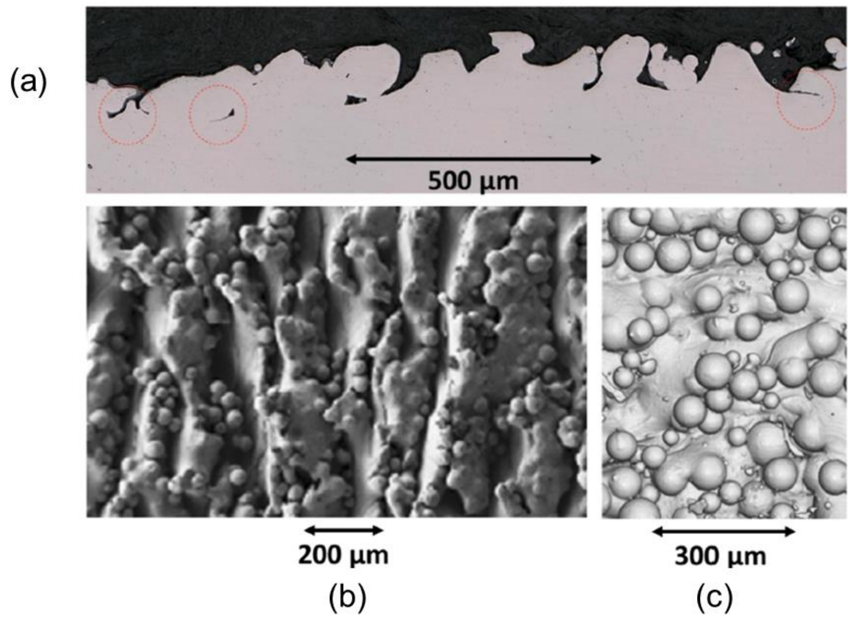

Figure 2-4

2.1.2 Post-AM Treatment

Among numerous post-AM treatment techniques, two types are of particular interest to this project are: Hot Isostatic Presssing (HIP) and surface machining /polishing. HIP has been shown effective for significantly reducing internal gas-entrapment induced porosities (particularly those in spherical shapes, e.g., Figure 2-3c) while surface machining /polishing is effective in reducing some of sharp protruded surface roughness features, as illustrated in Figure 2-4.

Hot Isostatic Pressing

HIP has been proven more effective in reducing internal porosities and improving overall mechanical properties than any other methods, as demonstrated by Zhang et al. [8] on stainless steel 316L. Figure 2-5 shows a comparison of the optical micrographs of samples under as-built, annealed at 982℃, annealed at 1093℃, and HIPing conditions. The effectiveness of HIP becomes less for interconnected or surface-connected porosities, as shown by Figure 2-6 (see Cegan et al [9]). This is a reason why Sanaei and Fatemi [2021] have observed from a large amount of fatigue test data that HIP yields insignificant improvement to fatigue lives for cracking originated from surface.

Machining/Polishing

Machine and polishing have been shown to offer some level of fatigue performance improvement, but the improvement is less noticeable in the low cycle fatigue (LCF) regime which is typically defined as cycles to failure less than 10^4 or 10^5, as given by Ziokowski et al. [10] for fatigue tests performed on stainless steel 304L (see Figure 2-7) and by Hatami et al. [11] on stainless steel 316L (see Figure 2-8).

In summary, various post AM processing effects on both internal and surface geometric discontinuities can be summarized in Figure 2-9 as described by Solberg and Berto [3].

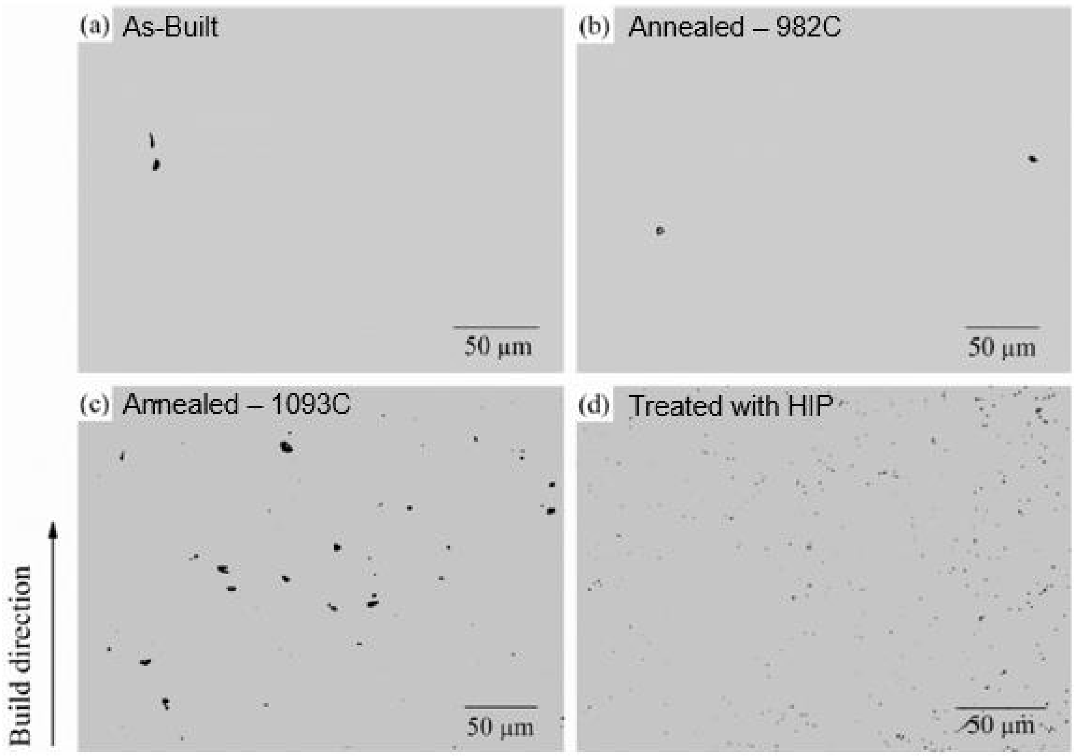

Figure 2-5

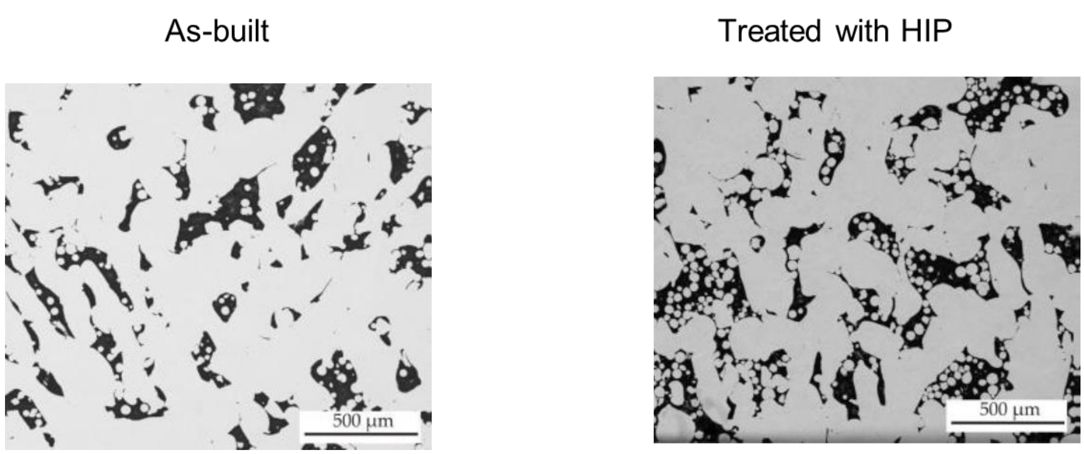

Figure 2-6

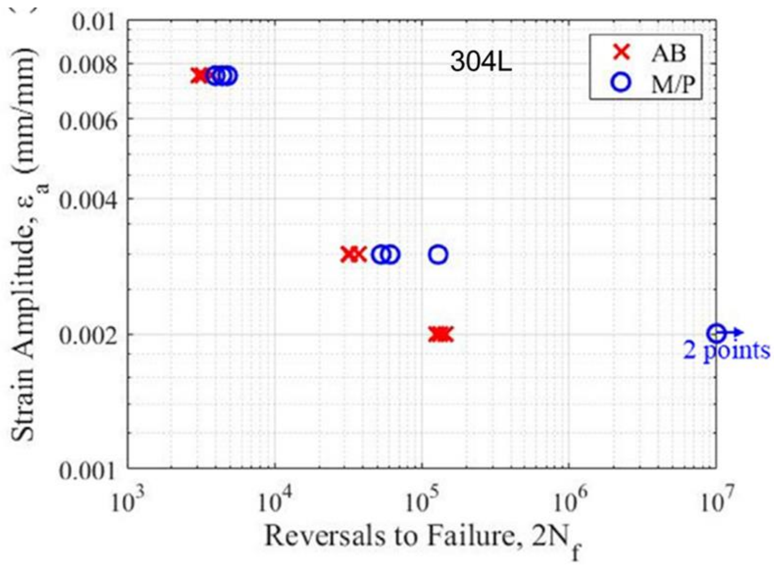

Figure 2-7

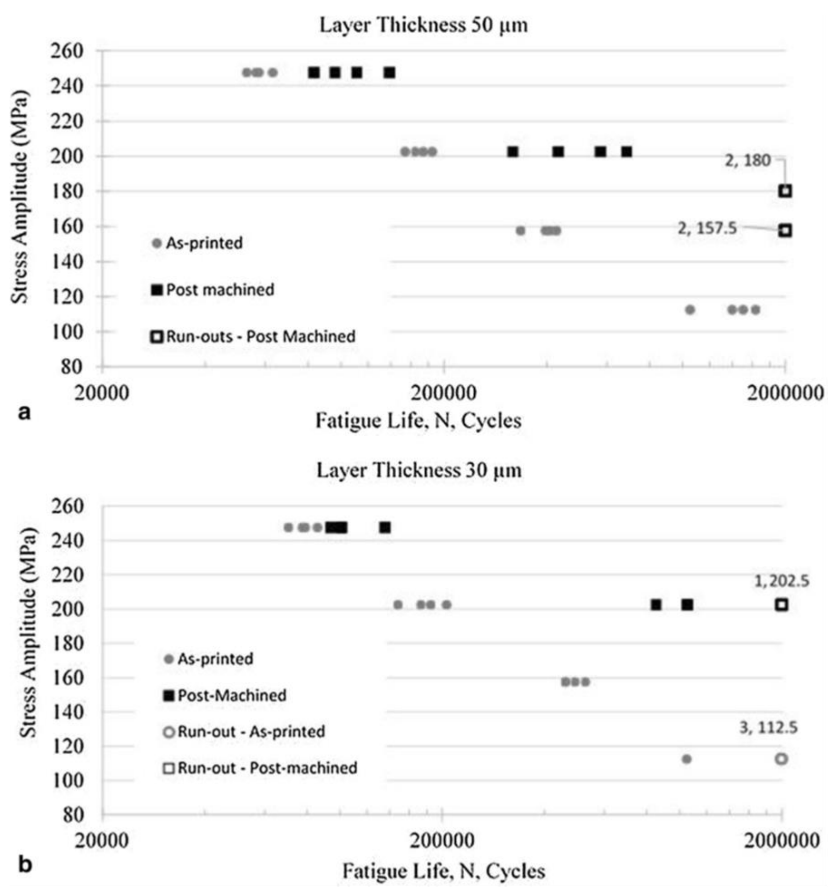

Figure 2-8

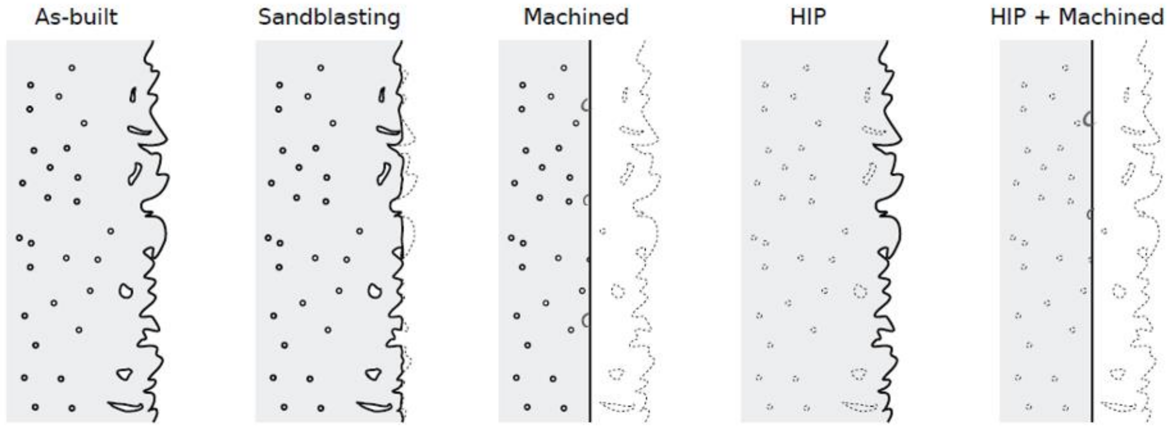

Figure 2-9

2.2 Assessment of distributed of defects and critical locations in AM components

Given the complex flaw distribution characteristics in AM components illustrated in Figure 2-9, any defect acceptance criteria to be developed needs to consider how multiple defects interact in contributing to structural integrity of a component. Existing flaw interaction criteria are mostly empirical in nature (as illustrated Figure 2-10, taken from BS 7910 which is the same as the criteria used in ASME XI) with limited cases of rigorous fracture mechanics evaluation for applications in welded components. These criteria tend to be excessively conservative, as demonstrated in Figure 2-11 by considering two coplanar elliptical flaws in a round bar AM specimen. The increase in stress intensity factor K due to actual flaw interactions is virtually unnoticeable versus an increase of about 40% if an equivalent flaw definition according to Figure 2-10 is used. The parametric analyses performed for this project shows that the interaction criterion in terms "s" can be reduced to $s \leq a_{min}$ where a_{min} represents the smallest of value between a_1 and a_2 in Figure 2-10.

Motivated by this finding, the rest of the parametric analysis can be done by considering a single equivalent defect of multiple discontinuities which satisfies the criteria described as $s \leq a_{min}$ in terms of their spacing s. As such, the effects of defect cluster location with a round bar section can be assessed as shown in Figure 2-12. The implications are as follows:

- There exists a critical region in which the effects of a cluster of geometric discontinuities can become significant
- This region (see Zone 1 in Figure 2-13) can be defined as a surface region within about 10% radius measured from surface
- For any defect cluster clusters situated further inside Zone 2 (see Figure 2-13), an equivalent defect size D can be more than twice as large to exhibit a similar stress intensity factor.

The above findings can be implemented in a cost-effective manner by considering critical locations in any pressure containing AM components by identifying critical locations in components, often referred to "hot spots", which will be addressed in the next section.

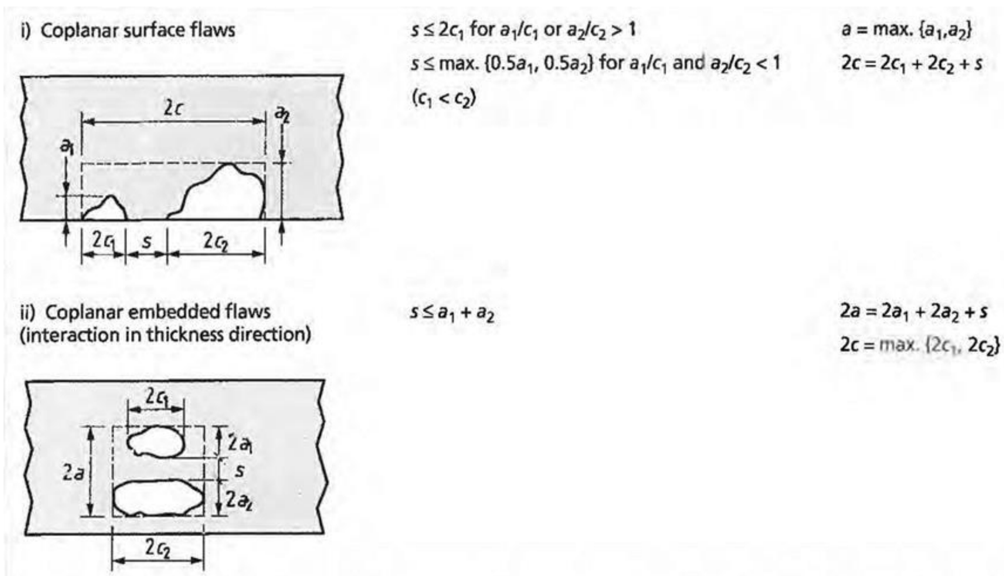

Figure 2-10

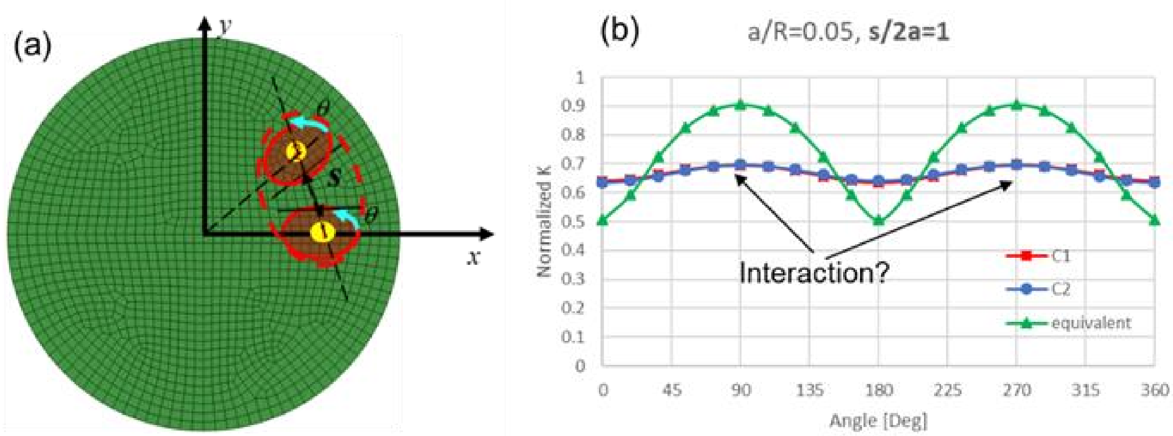

Figure 2-11

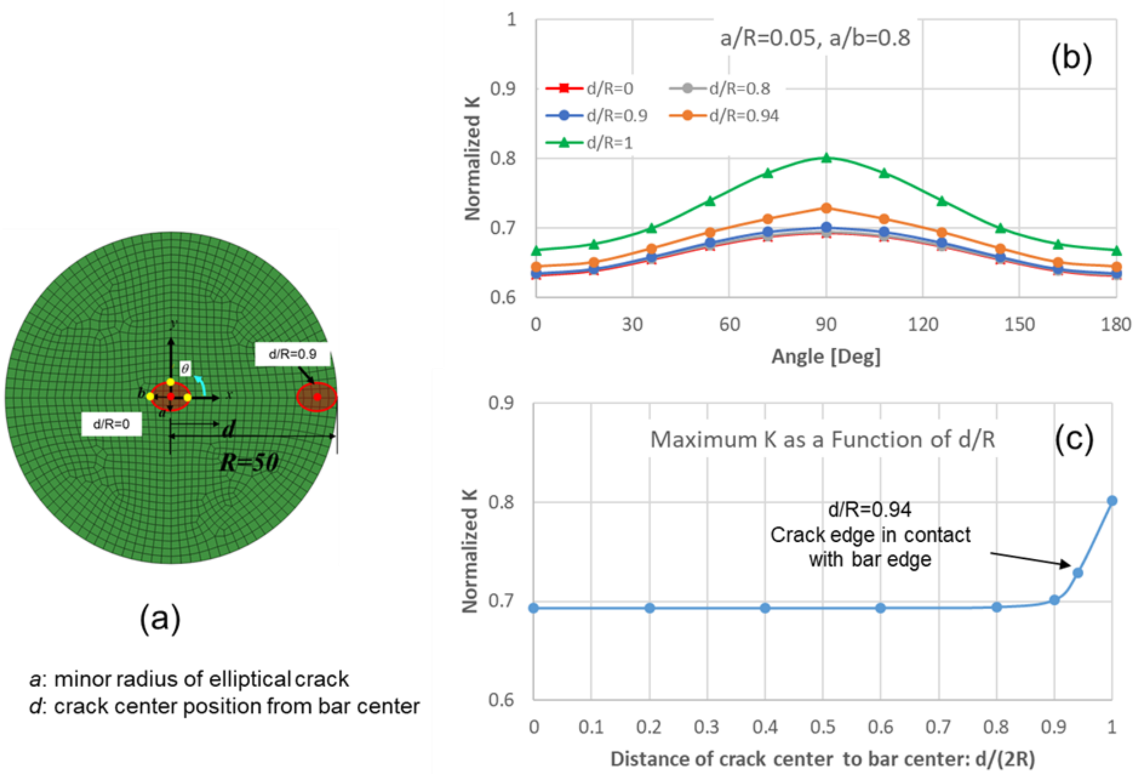

Figure 2-12

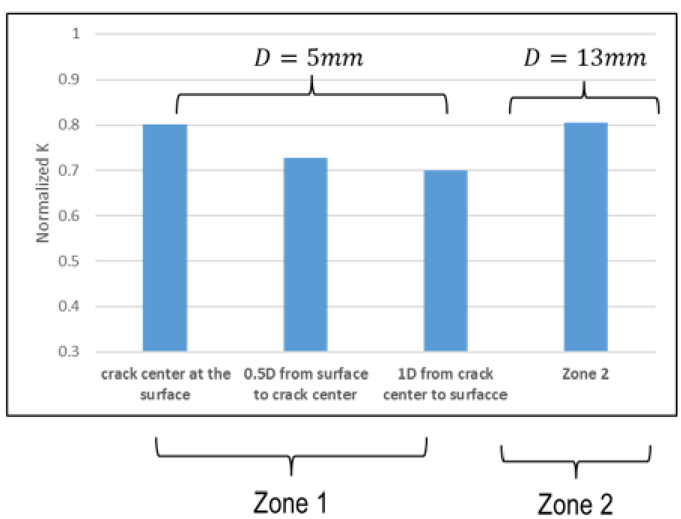

Figure 2-13

2.3 Critical Locations in AM Components

A total of four components have been identified for evaluation of hot spots so that effective quality acceptance criteria can be cost-effectively implemented according to the findings established in the above section (Sec. 2.2.1). These components are illustrated in Figure 2-14. The components will be analyzed by means of the mesh-insensitive structural stress method adopted by ASME Div 2 [12].

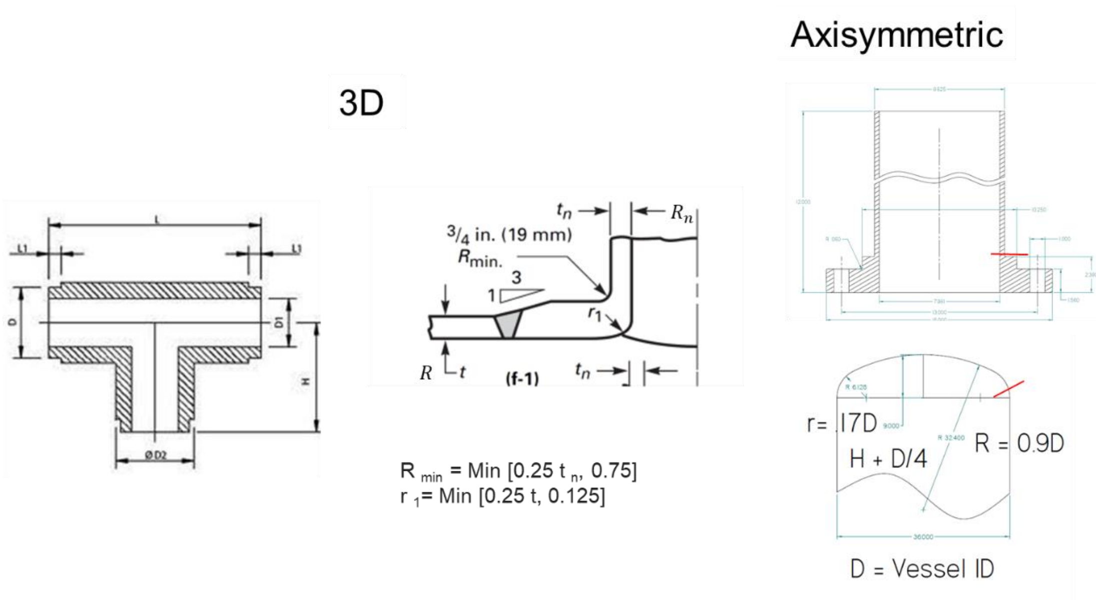

Figure 2-14

2.3.1 Pipe T Connection

A shell element model was used, as shown in Figure 2-15. The structural stress (through thickness membrane plus bending) results along the intersection both for any fatigue cracking development into the main pipe (A-A) with a larger diameter and into the branch pipe (B-B) are considered, as shown in Figure 2-16. As can be seen, in both cases, crown locations are the critical locations showing highest structural stresses while saddle positions exhibit the secondary highest positions under unit internal pressure loading. For the latter, the saddle positions can become the most critical locations if the branch pipe is loaded in tension along the branch pipe axial direction.

To further examine the structural stress distribution on the main pipe as a function of distance from the crown position, Figure 2-17 shows the normalized axial structural stress rapidly decreases to about a value of 3 at a normalized distance of $0.25\sqrt{RT}$, where R and T are main pipe radius and wall thickness, respectively. Therefore, the critical region on the main pipe can be defined as from the crown position to an axial distance of $0.25\sqrt{RT}$ for quality control purpose. The same observation can be made for the critical location at crown position but situated on the branch pipe, as shown in Figure 2-18.

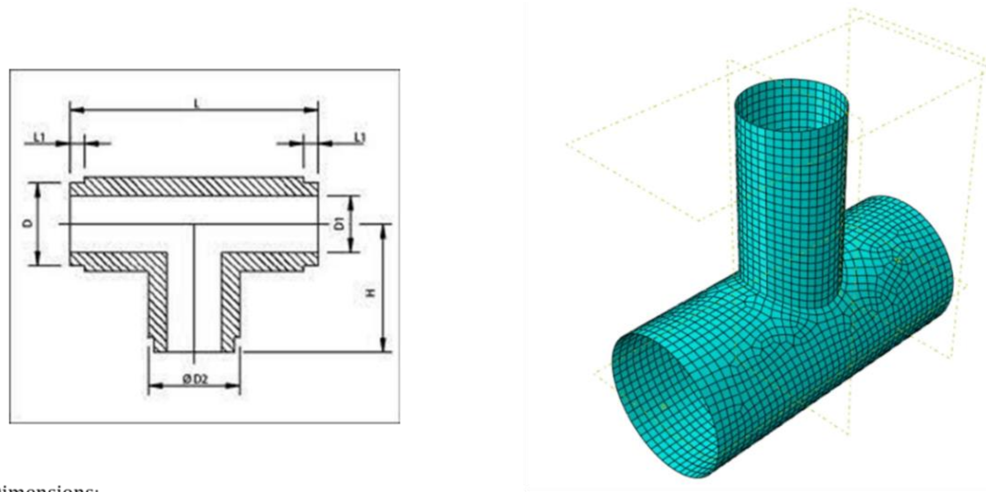

Dimensions:

$\frac{R_1}{t} = 15\,; \frac{R_2}{t} = 10; D = 93\text{mm}; D_1 = 87\text{mm}; D_2 = 63\text{mm}$

Loading: unit pressure with end cap effects

Statically determinate BC's at branch end

Figure 2-15

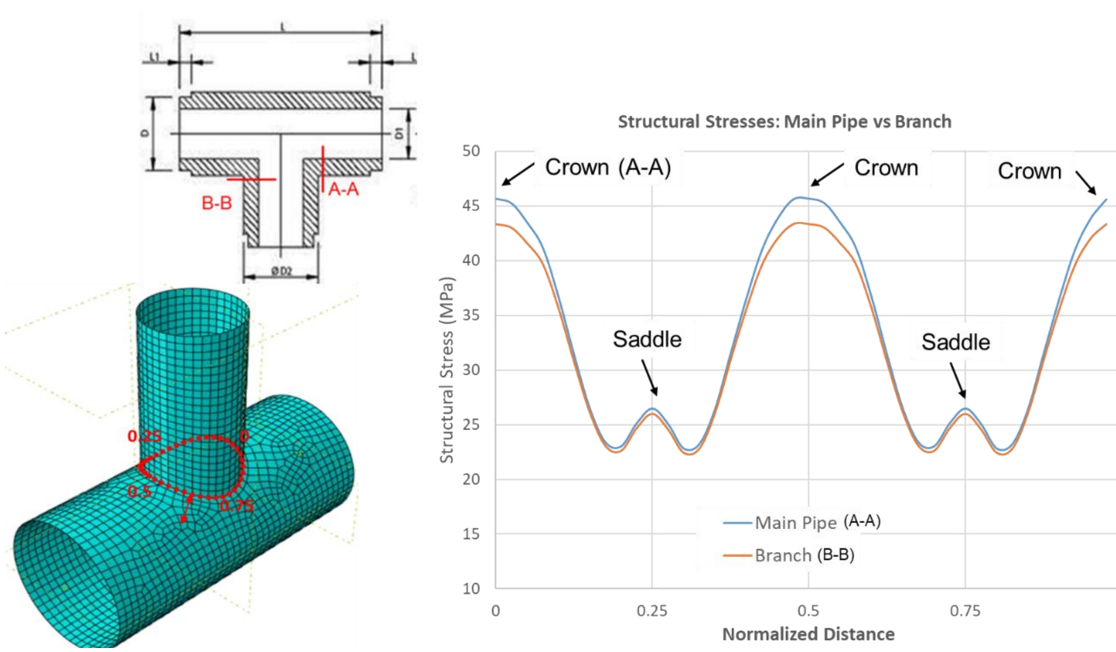

Figure 2-16

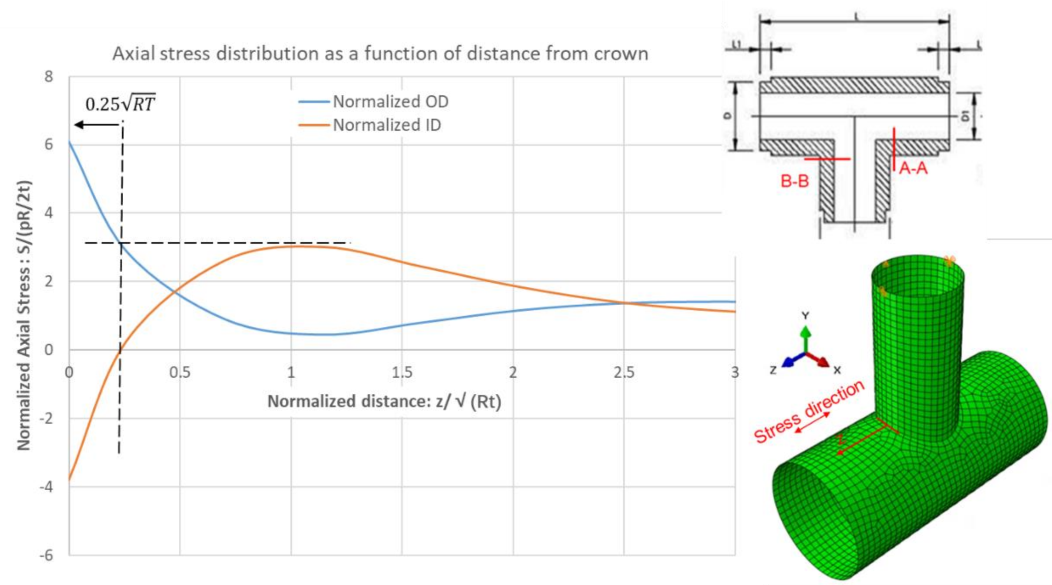

Figure 2-17

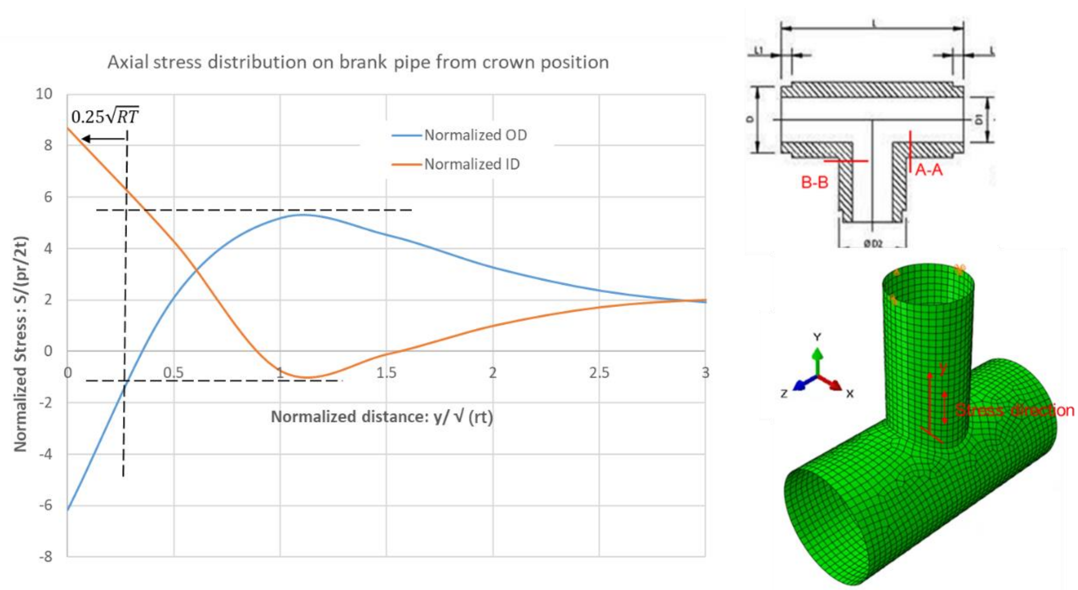

Figure 2-18

2.3.2 Self-Reinforced Nozzle

The self-reinforced nozzle represents some complexity for parametric structural stress modeling if 3D solid element model is used (see Figure 2-19). However, the traction structural stress method has been proven effective to model similar 3D components using a shell element model for which various geometric parameters can be readily changed for performing a large number of parametric analyses.

For demonstrating the adequacy of shell element models, an axisymmetric reinforced padding area was first considered to demonstrate the consistency of the structural stress results between shell element and 3D solid element results (see Figure 2-20).

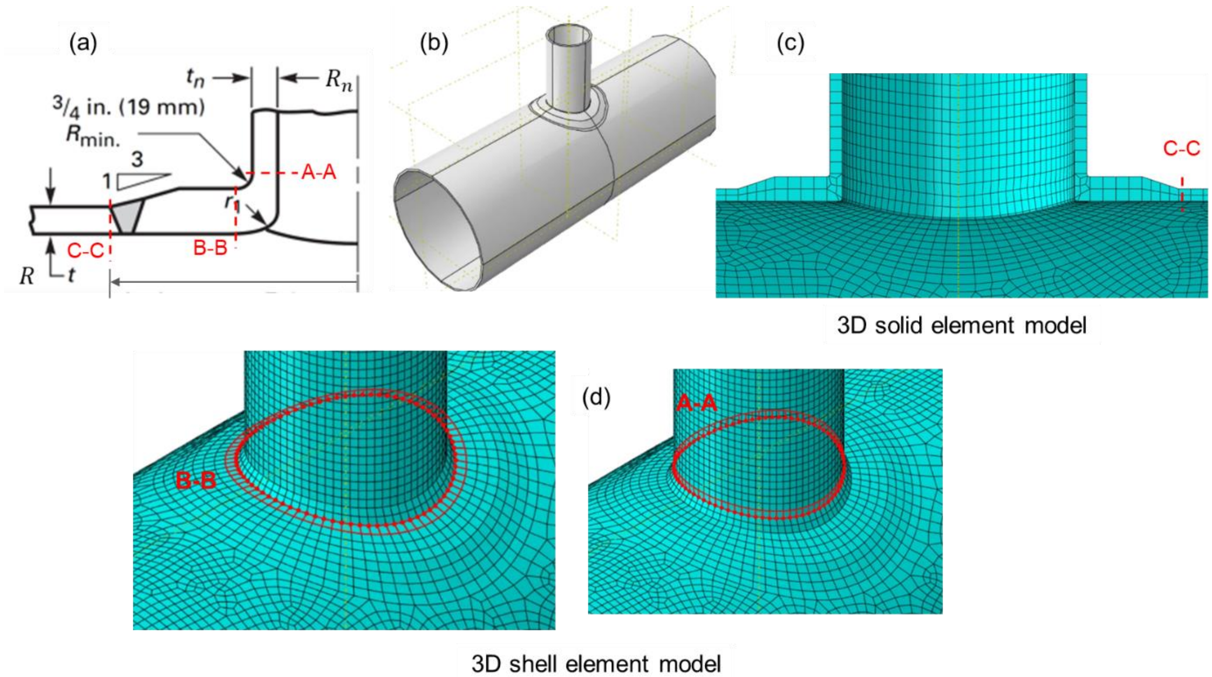

Figure 2-19

The axisymmetric shell element and 3D solid element of models with the reinforced padding are shown in Figure 2-20a, subjected to the same pressure loading conditions. The structural stress results along the intersection between the tapered reinforced padding and main plate are compared in Figure 2-20b, indicating the results are the same between the shell element and 3D solid element models. As a result, the shell element model shown in Figure 2-19 will be used from this point on.

There are additional dimensions that need to be introduced for defining the size of the reinforced nozzle padding size. After consulting with the project representative at SRNL, the presentation by R. Ferell (2019) [13] is used as a reference, as shown in Figure 2-21. Of a particular interest for this investigation is the dimension definitions encircled in Figure 2-21, where the nozzle reinforcement size d can be determined as:

$$d = \max\left\{\left(\frac{D_p}{2}+s\right),\left(R_n+t_n+t\right)\right\} \tag{2.1}$$

For the reinforced nozzle geometry sketch given in Figure 2-19, the following dimensions are chosen for the present hot spot investigation efforts:

$$\frac{R}{t} = \frac{R_n}{t_n} = 10$$

$t = 9.15mm$; Reinforced area $t_R = 1.33t$

in which t_r represents the thickness of the reinforced padding. According to Figure 2-19, the above dimensions leads to:

$d = 57mm$ or $40.65mm$

For comparison purposes, both $d = 57mm$ and $d = 40.65mm$ will be considered in this investigation.

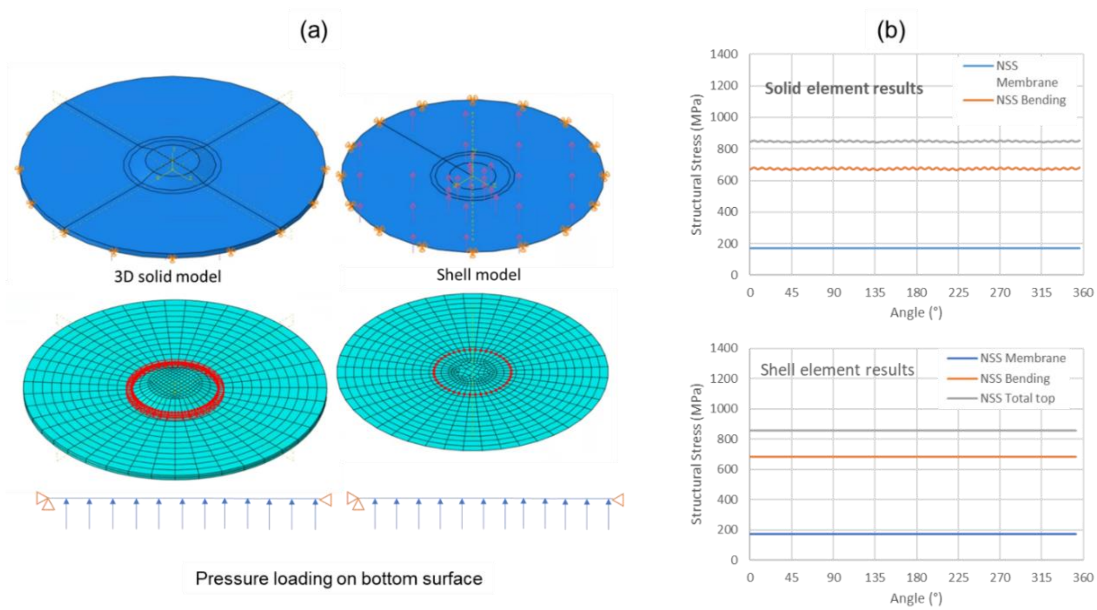

Figure 2-20

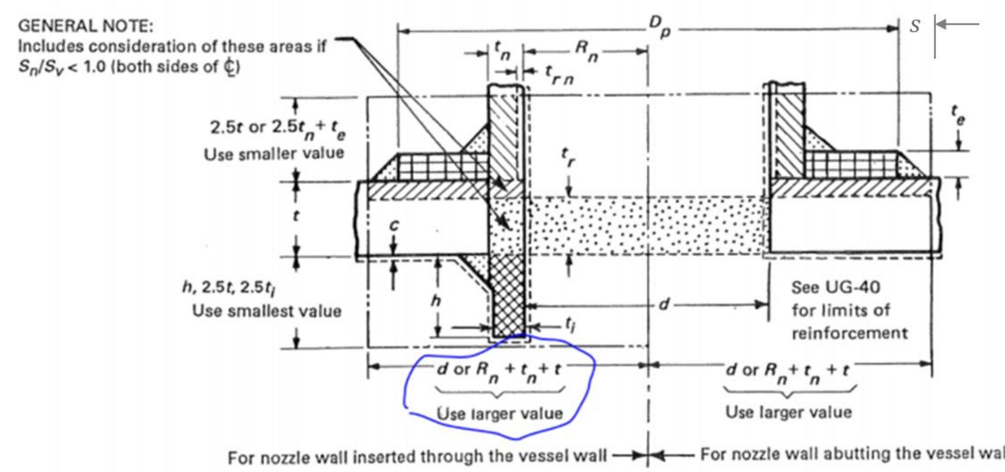

Ref: R Ferrell (2019)

Figure 2-21

Case 1: $d = 57mm$:

The structural stress results along three through-thickness sections, A-A, B-B, and C-C are summarized in Figure 2-22. Note that the structural stresses normal to the three through-thickness planes are labeled as “M+B” (i.e., membrane + bending parts) and the structural stress in shear acting on those plane along the circumferential direction are labeled as “Tau_M+B” (see detailed discussions in [14]). The saddle positons correspond to 90° and 270°, while crown positions correspond to 0° and 180°, respectively. It can be seen that both crown positions serve as hot spots at Section A-A while saddle positions at Section C-C. Due to the presence of the self-reinforcement with an increased thickness, Section B-B exhibits a more uniform normal structural stress distribution with the self-balancing shear structural stress being comparable in magnitude within the regions between saddle and crown positions. The results in Figure 2-22 suggests that crown positions along A-A requires special attention in quality control during AM fabrication of such components.

Case 2: $d = 40.65mm$:

By considering the lower value of $d = 40.65mm$ according to Eq. (2.1), the structural stress results are shown in Figure 2-23. Although the overall results are rather similar to those shown in Figure 2-22, it is important to note the structural stress results at critical locations along Sections A-A and C-C are noticeably reduced. This suggests that Eq. (2.1) given in [13] should be re-evaluated, which is beyond the scope of this project.

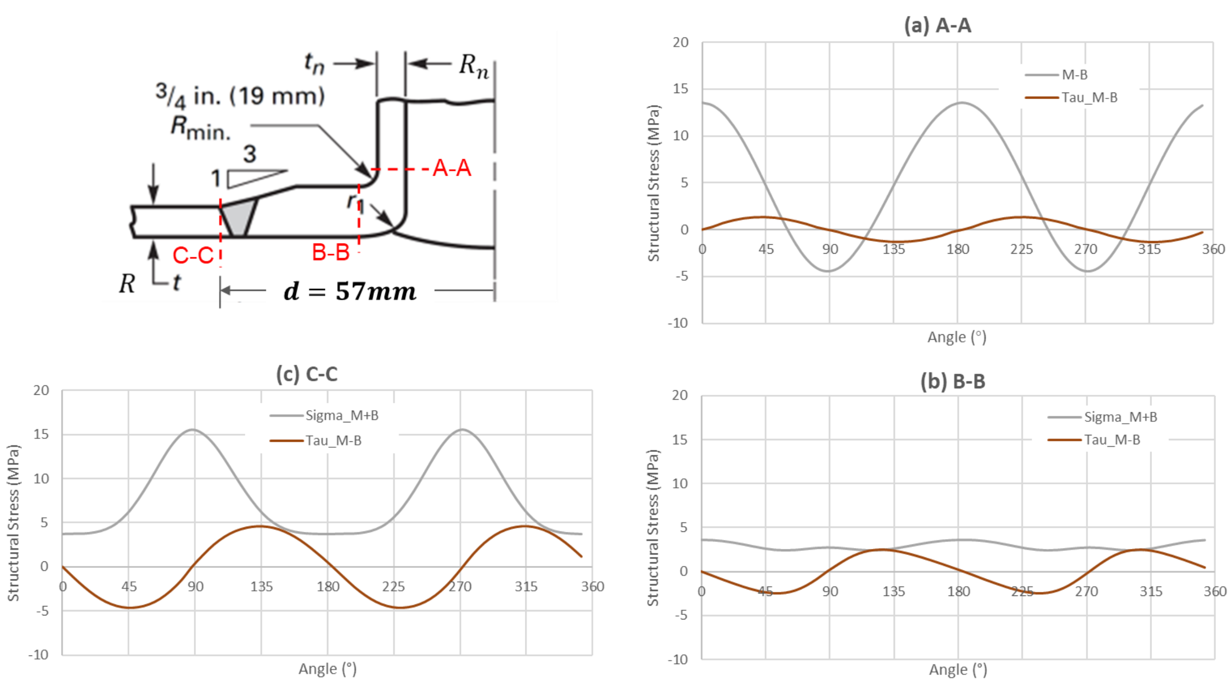

Figure 2-22

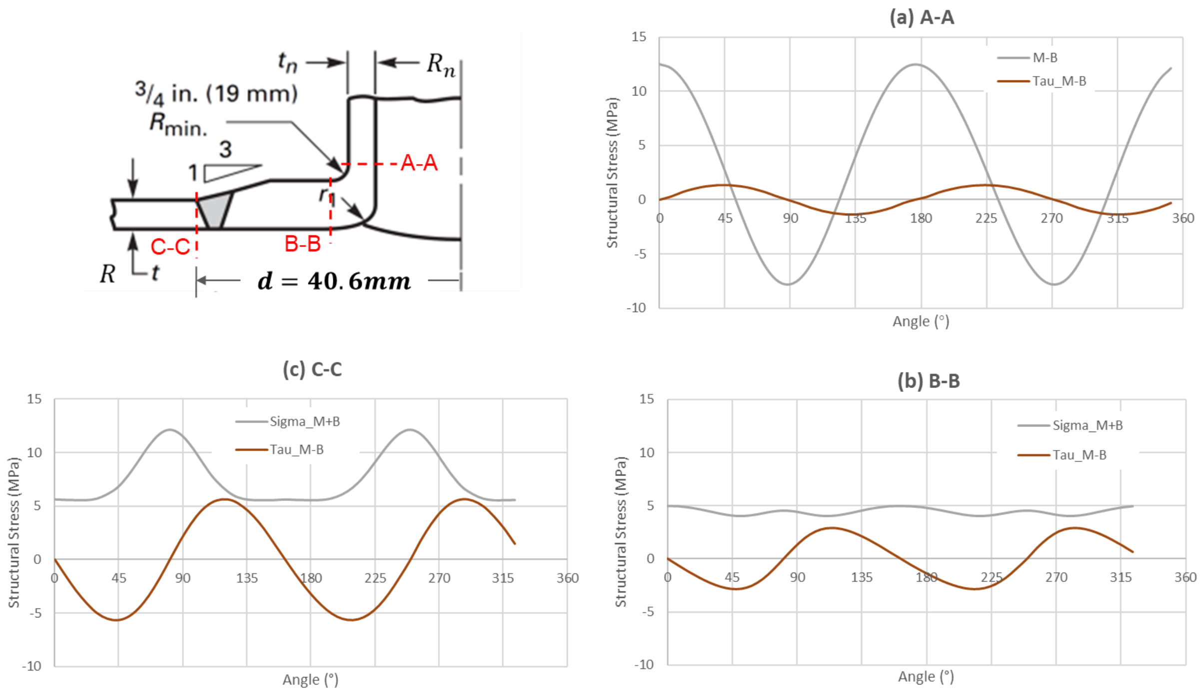

Figure 2-23

2.3.3 Pipe Flange

The flange geometry is given in Figure 2-24a. Two pipe section lengths (l) are investigated to demonstrate that there exists a minimum length around 2-3$\sqrt{Rt}$ [15] in the AM pipe flange design, beyond which the resulting stress concentration at its critical location should remain the same. Knowing this minimum length is important for reducing AM cost.

By inspection, the critical location under either internal pressure or external pipe bending should be located the through-thickness cross-section A-A shown in the axisymmetric FE model in Figure 2-24b. By considering end cap effects, normal structural stress based stress concentration factors (SCF) with respect to the normal stress (i.e., pR/t) are summarized in Figure 2-25.

The structural stress based SCF results summarized in Figure 2-25 indeed show that a pipe section $l = 2\sqrt{Rt}$ or $8.3\sqrt{Rt}$ given in Figure 2-24a) yields essentially the same SCF value, suggesting the pipe section can be reduced to $2\sqrt{Rt}$ for reducing AM cost. The results in Figure 2-25 also suggest Section A-A requires special attention in quality control, since this area is subject significantly higher bending stresses.

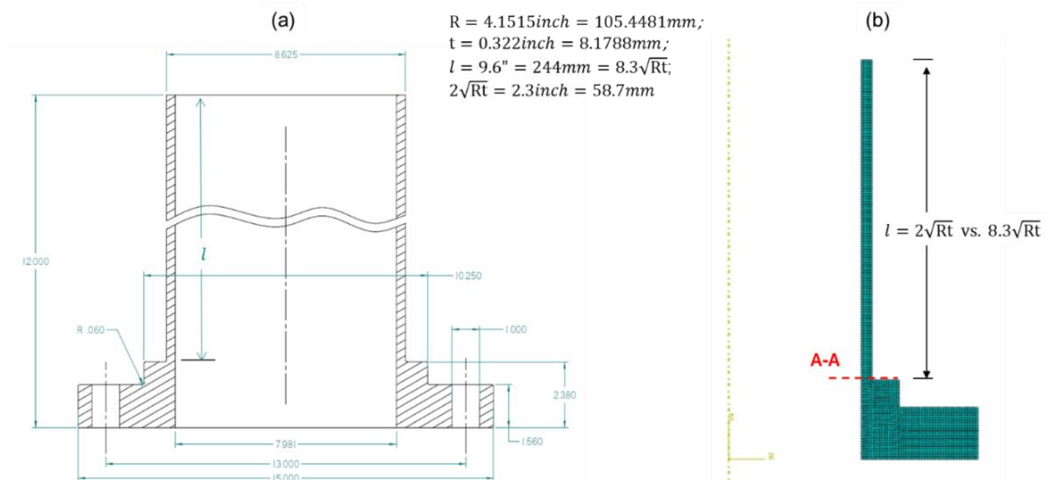

Figure 2-24

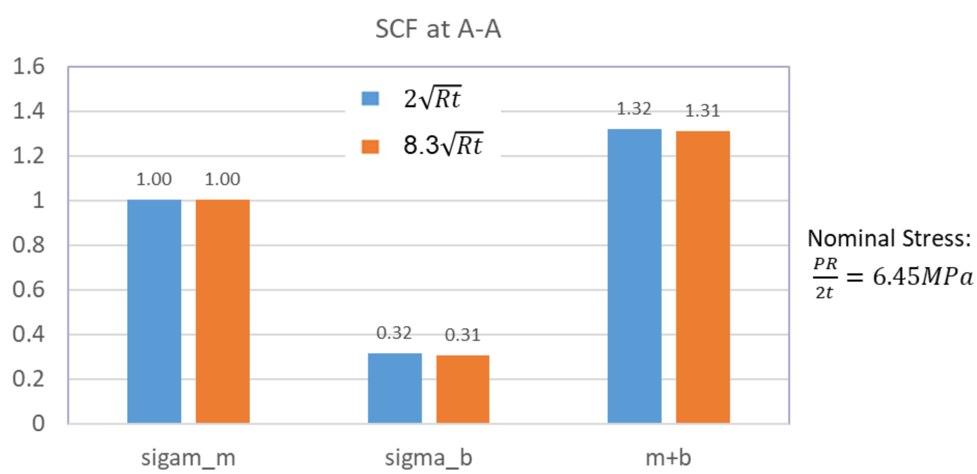

Figure 2-25

2.3.4 Elliptical Head

The elliptical head geometry is described in Figure 2-26a. Its axisymmetric FE model for structural stress computation is shown in Figure 2-26b. It is well known that high stress regimes should be located in the curved head section.

The structural stress normal to θ plane shown in Figure 2-27a as θ varies from $0°$ to $90°$ are searched and summarized in Figure 2-27b corresponding to internal pressure loading of unity and in Figure 2-27c in terms of SCF with respect to $pR/2t$ of the cylindrical vessel section. It can be seen the highest SCF of 3.16 occurs at about $45°$. The results suggest that a region of high stress region can be defined within about 25° to 60° may be considered for quality control purpose in AM fabrication of such elliptical head components.

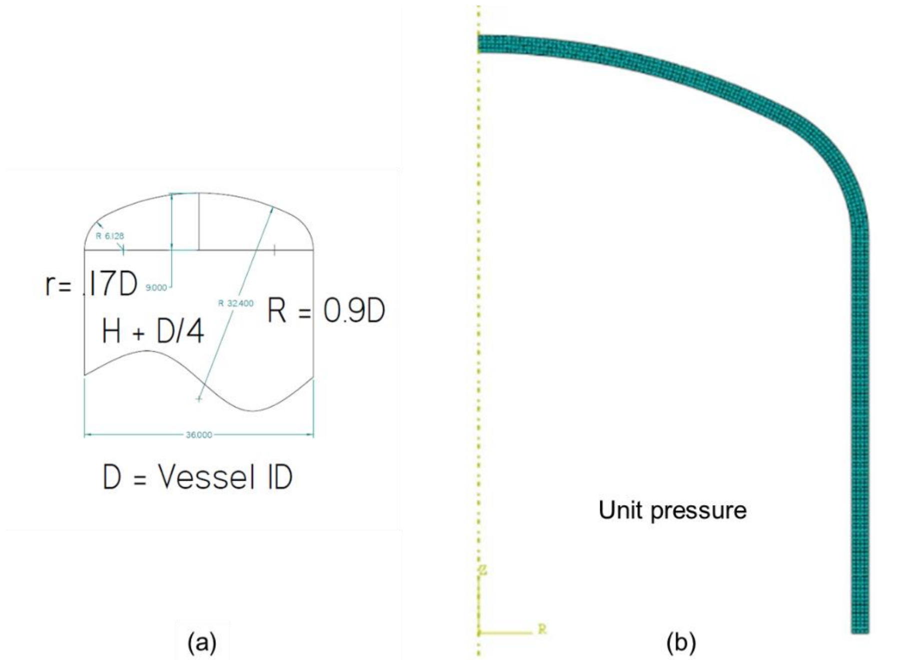

Figure 2-26

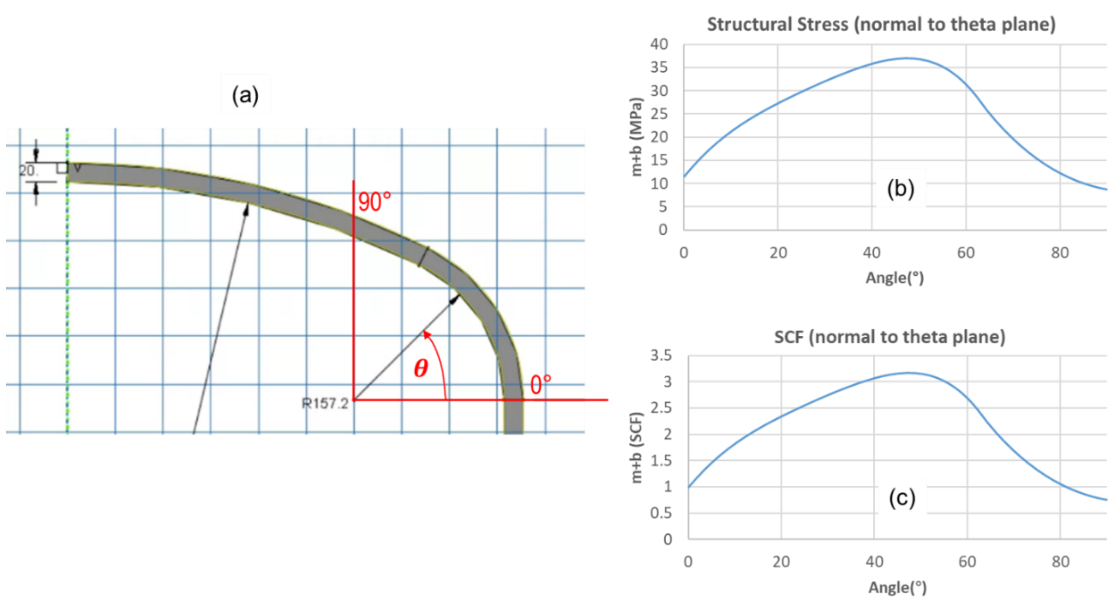

Figure 2-27

2.4 Fatigue data analysis and master S-N and E-N curve correlation

2.4.1 Mechanics Basis

It is well known that the most dominant effects of geometric discontinuities summarized in Figure 2-1 through Figure 2-3) are on fatigue properties. AM fatigue test data obtained on notched specimens have been analyzed to examine what existing analysis technique should be considered for AM component fatigue analysis. The well-documented test data on Inconel 718 AM specimens from Solerg and Berto (2019) were analyzed using the mesh-insensitive structural stress method adopted by ASME Section VIII Division2 [12]. The specimens evaluate are shown in **Figure 2-28**a and the finite element models used in this study are given in **Figure 2-28**b. The structural stress range parameter Eq **Error! Reference source not found.** is effective in correlating the S-N data regardless of notch geometry conditions given in **Figure 2-28**a. In addition, the AM data fall into the ASME Section VIII Division 2 master S-N curve scatter band, as shown in **Figure 2-28**c. This finding shown in **Figure 2-28**c is important in that the master S-N curve approach can be used to correlate available stainless steel AM data, which will greatly simplify fatigue design procedure, as long as current ASME flaw acceptance criteria are met.

Encouraged by the findings shown in **Figure 2-28**c, a comprehensive literature search on fatigue test data on stainless steel 304L and 316L was conducted focusing on test data from notched specimens.

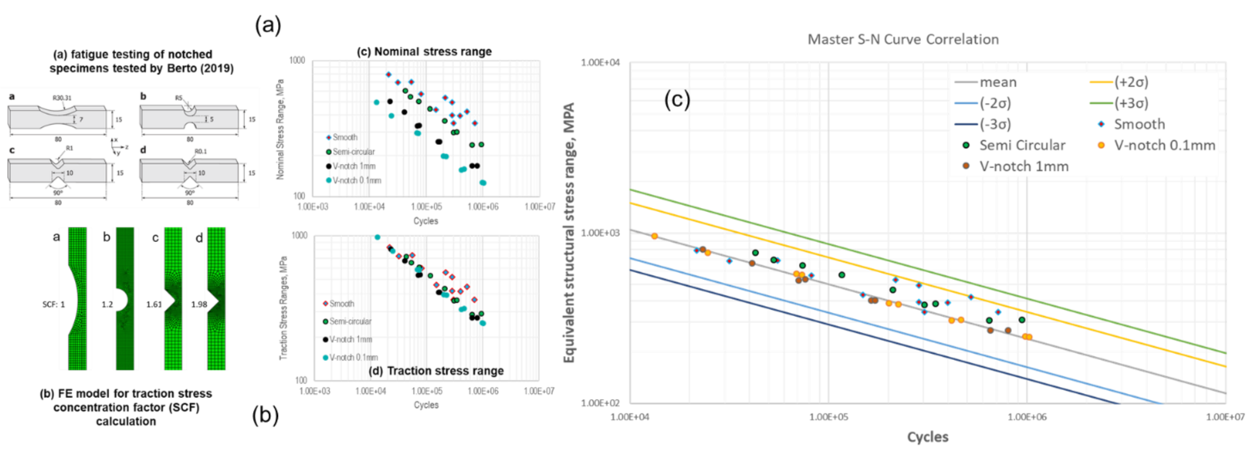

Figure 2-28

2.4.2 Master S-N/E-N Curve for AM Components

An overview of the structural stress method in ASME BP&V Div 2 Code [12] is outlined below. The structural stress based master S-N curve is given by Eq. **Error! Reference source not found.** which led to the development of the master S-N curve by effectively correlating about 1000 full scale and large scale fatigue tests of welded components [12].

$$\Delta S_s = \frac{\Delta\sigma_s}{t^{\frac{2-m}{2m}} \cdot I(r)^{\frac{1}{m}}} \qquad (2.2)$$

The thickness term t represents weldment thickness in ASME BP&V Div 2 Code [12] when fatigue cracking is assessed. For AM specimen data correlation, t can be interpreted as an equivalent thickness in fatigue crack growth direction in AM fatigue specimens. For those specimens shown in Figure 2-28a, $t_e = w/2$ where w is specimen width at the notched section. If round bar AM specimens are considered, $t_e = d/2$, in which d is the diameter of round bar fatigue specimens used. In addition, in Eq. **Error! Reference source not found.**), $m = 3.6$, based on crack growth rate analysis of well known da/dN versus ΔK data [16] and $r = \Delta\sigma_s/\Delta\sigma_b$ for the dimensionless life integral $I(r)^{\frac{1}{m}}$ is given in Eq. (2.3) below,

$$\begin{aligned} I(r)^{\frac{1}{m}} &= 0.0011 \cdot r^6 + 0.0767 \cdot r^5 - 0.0988 \cdot r^4 + 0.0946 \cdot r^3 \\ &+ 0.0221 \cdot r^2 + 0.014 \cdot r + 1.2223 \end{aligned} \tag{2.3}$$

based on a best-fit of numerical integration results under load-controlled test conditions, and

$$\begin{aligned} I(r)^{\frac{1}{m}} &= 2.1549 \cdot r^6 - 5.0422 \cdot r^5 + 4.8002 \cdot r^4 - 2.0694 \cdot r^3 \\ &+ 0.561 \cdot r^2 + 0.0097 \cdot r + 1.5426 \end{aligned} \tag{2.4}$$

under displacement-controlled conditions.

Eq. **Error! Reference source not found.**) can be directly concerted to equivalent structural strain range by dividing $\Delta\sigma_s$ by material Young's modulus *E*, as:

$$\Delta \mathrm{E}_s = \frac{\Delta \varepsilon_s}{t^{\frac{2-m}{2m}} \cdot I(r)^{\frac{1}{m}}} \tag{2.5}$$

The significance of Eq. (2.5) lies in the fact that it can be used for low cycle fatigue (LCF) evaluation of welded components regardless of metal or alloy types, as long as they are welded [17], in addition to high cycle fatigue (HCF). Eq. (2.5) will be used from this point for its generality.

2.4.3 AM Fatigue Test Data Analysis – Stainless Steel

Over 150 publications and reports containing AM specific fatigue test data or their analysis on stainless steel 304L or 316L have been reviewed during this project. Among these publications, those containing complete documentations so that detailed evaluations can be performed are summarized in Table 1 [3, 6, 18-21]. Note that more details on these fatigue tests and data on other AM materials are given in Appendix A.

Table 1: AM Fatigue Data Sources and Test Details

Source and Material	E - Wrought	*t* or *d* (mm)	Surface conditions	LC vs. DC - l(r)	R	Specimen Type
Berto (2019) - IN 718	208GPa	2.5 & 3.5	As-built	Load control	0	Notched bar
Brenne (2019) –SS 316L	193GPa	1.5	As-built	Load control	0.1	Notched plate
Smith et al.(2019), SS 304L	193GPa	4.0	As-built	Load control	0.1	Notched bar
Shrestha (2021) – SS 316L	193GPa	4.76 &4.8	As-built	Load control	-1	Smooth bar
Shrestha (2019) – SS 316L	193GPa	3.5	As-Built vs M/P	Disp-control	-1	Smooth bar
Zhang (2017) – SS 316L	193GPa	3	EDM	Load control	0.1	Smooth plate
EPRI report – SS 316L	195GPa	15.875	HIP	Disp. control	-1	Smooth bar

The corresponding specimen types involving stress concentration effects are given in Figure 2-29. The specimens used in EPRI's tests are not shown in Figure 2-29 since it is not given in the EPRI report [21] evaluated in this investigation. For all specimens containing notch effects, structural stress analyses were performed to determine the structural stress and structural strain based stress concentration factors.

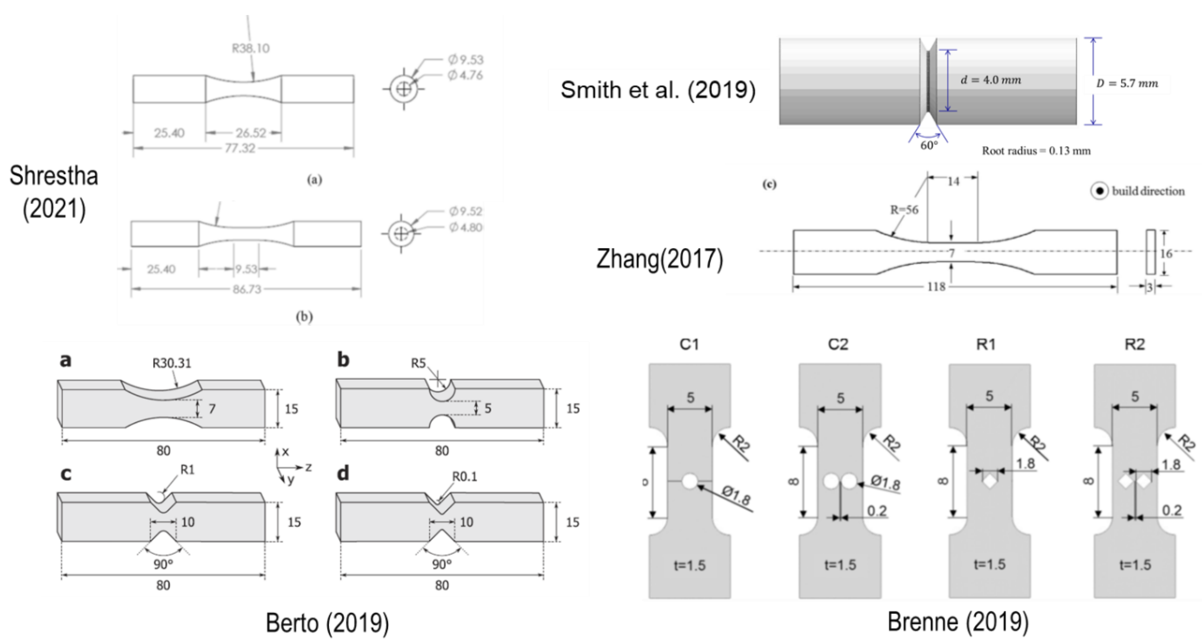

Figure 2-29

As shown in Figure 2-30, the equivalent structural strain range parameter given in Eq. (2.5) provides an effective means for correlating all the test data analyzed into a single correlated band for all the various types of specimens and testing conditions considered as shown in Table 1. More importantly, all the test data seem to show a reasonable correlation with the master E-N curve scatter band used in ASME

Div 2 for welded components. Without using structural strain based parameter for different materials (or structural stress based for similar materials), the resulting data scatter band would be much larger, as shown in **Figure 2-28**a in which the nominal stress range was used, even if the four data sets were from the same Inconel 718 AM material were considered.

It is important to note that displacement-controlled test data by EPRI [21] are situated somewhat above the upper bond (mean + 3σ) in Figure 2-30 and while those by Shrestha et al. [22] are situated slightly below the lower bond (mean - 3σ). The difference may be attributable to different failure criterion used. The former used the final specimen rupture by EPRI [21] while the latter used 50% load by Shrestha et al. [22]. Further evaluation on this will be carried out once more data under displacement controlled conditions become available.

There is a great deal of debates in the recent literature on any significant differences in fatigue properties between as-built and machined/polished (M/P) conditions if microscopic level discontinuities are similar. This question may be addressed by examining the strain-controlled data by Shrestha et al. [22], as shown in Figure 2-31. The fatigue test data seem to show machined/polished tend to be situated in the upper scatter band in the high cycle regime with cycles to failure beyond 10^4 cycles. Below 10^4 cycles which there seems no clear trend. This data trend is also confirmed by other authors [6,10,11] (see also Figure 2-7 and Figure 2-8) for other metals, e.g., Inconel 718, Ti- 6-4, and aluminum alloys.

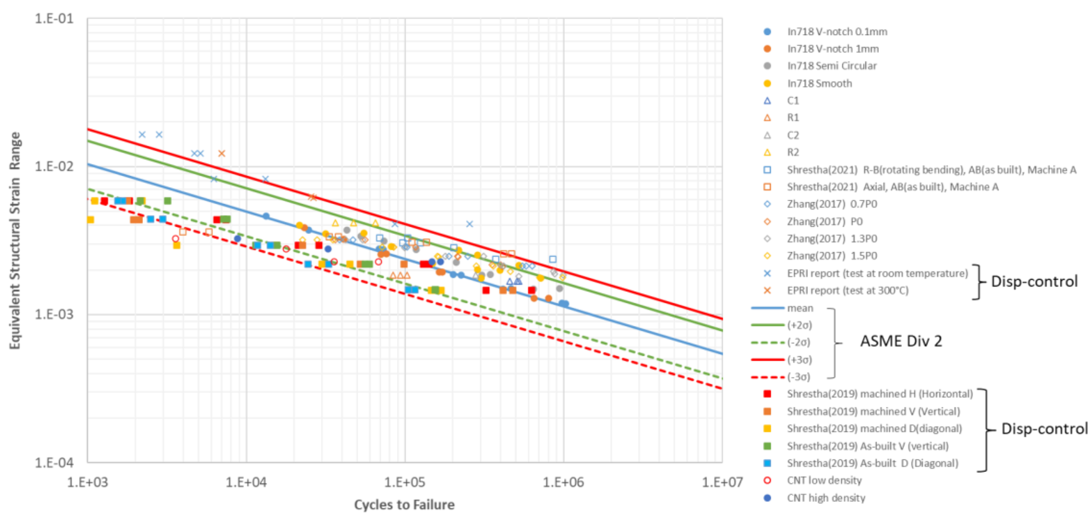

Figure 2-30

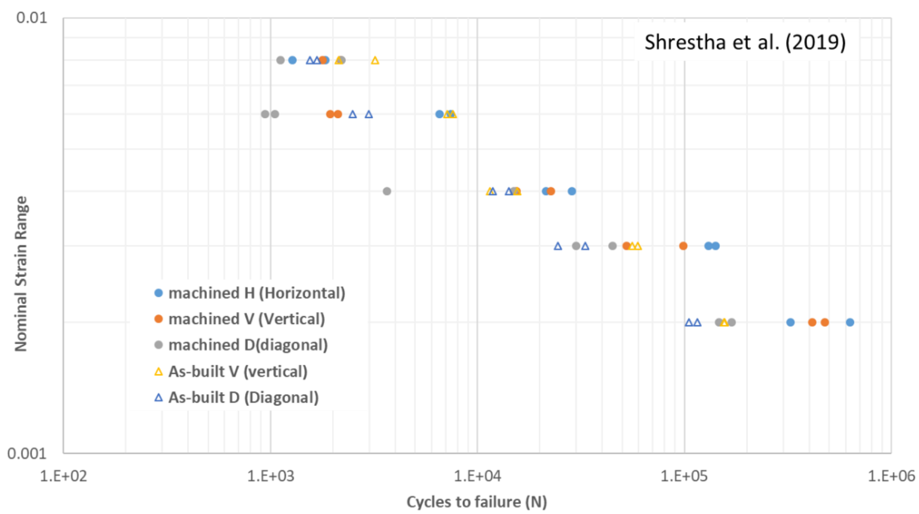

Figure 2-31

2.4.4 AM Fatigue Test Data Analysis - Other Materials

During the second year of this project, it was decided to expand the AM fatigue test data collection by considering Inconel, Ti-6-4, and aluminum alloy for comparison purposes. In this process, all test data collected and analyzed, including those summarized in Table 1, Figure 2-29 and Figure 2-30, are documented in detail as documented in Appendix A for traceability and future reference.

To demonstrate the effectiveness of Eq. (2.5), Figure 2-32 shows the comparison of the test data in Figure 2-30 (shown as gray symbols here) and newly collected test data (shown as colored symbols) for Ti-6-4, Inconel 718, aluminum alloy (AlSi10Mg). Again, a good overall correlation with the ASME Div 2 master E-N curve scatter band (lines) can be seen in Figure 2-32.

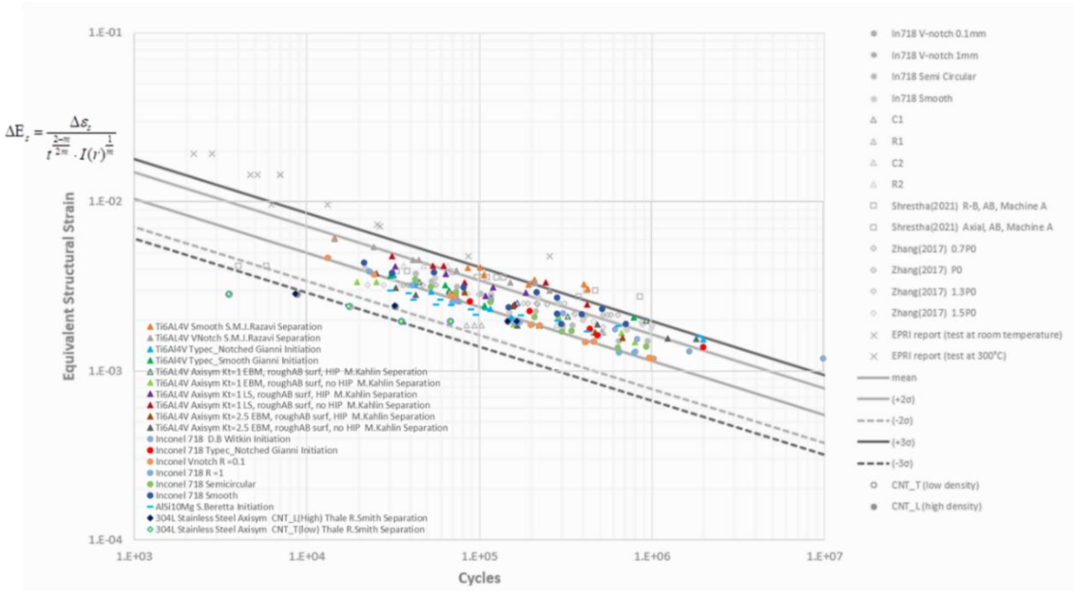

Figure 2-32

2.4.5 Master E-N Curve Representation of AM Test Data

Up to this point, the AM test data correlation in the form of master E-N curve (see Figure 2-30 and Figure 2-32) was based on Young's moduli reported by individual authors, either through their own testing or from various handbook sources. In this section, the Young's moduli stipulated in ASME Sec. II Code are used, as summarized in Table 2.

Table 2: Young's Moduli Stipulated in ASME Code

Modulus of Elasticity E = Value Given × 10E3 Mpa																		
									Temperature°C									
		−200	−125	−75	25	100	150	200	250	300	350	400	450	500	550	600	650	700
304L SS	UNS 30403	209	204	201	195	189	186	183	179	176	172	169	165	160	156	151	146	140
										Temperature°C								
Inconel 718	UNS 07718	−200	−125	−75	25	100	150	200	250	300	350	400	450	500	550	600	650	700
		214	210	206	199	195	192	190	188	185	183	180	176	173	169	…	…	…
					Temperature°C													
		25	100	150	200	250	300	350	400									
Ti6AL4V	Estimate	107	103	101	97	93	88	84	80									

The resulting master E-N curve representation of all test data documented in Appendix A is given in Figure 2-33, in which the scatter band is given in terms of mean $\pm 2\sigma$ and $\pm 3\sigma$. The scatter band represents the standard deviation of 0.37. The slope is at $-1/3.1$. Note that low density test data shown in Figure 2-32 are not considered here since their quality conditions would be screened out by the quality criteria currently being considered by BPTCS/BNCS committee. By comparing with ASME Div 2 master E-N curve and its background data (see Figure 2-34), the standard deviation of the AM test data still relatively large, mostly contributed by the ultrasonic frequency AM test results in the regime 10^6 to 10^8, which requires further examinations in the near future. In addition, the most of other AM test data in Figure 2-33 are clustered between 10^4 to 10^6 cycles to failure while ASME weldment test data spans between 10^2 to 10^8 cycles to failure. To increase the reliability in deriving fatigue design stress allowable, more reliable test data both below 10^4 and beyond 10^6 should be a focus of future investigations.

$$\Delta E_s = \frac{\Delta \varepsilon_s}{t^{\frac{2-m}{2m}} \cdot I(r)^{\frac{1}{m}}}$$

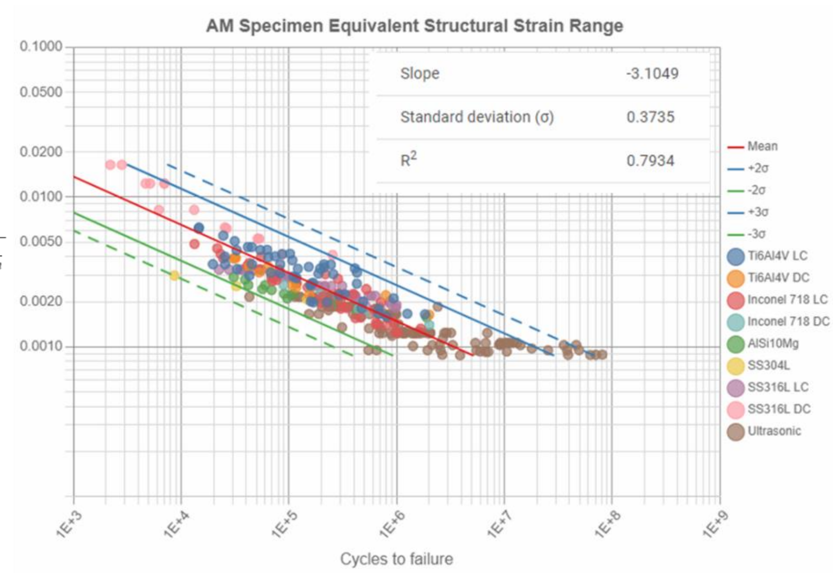

Figure 2-33

$$\Delta E_s = \frac{\Delta \varepsilon_s}{t^{\frac{2-m}{2m}} \cdot I(r)^{\frac{1}{m}}}$$

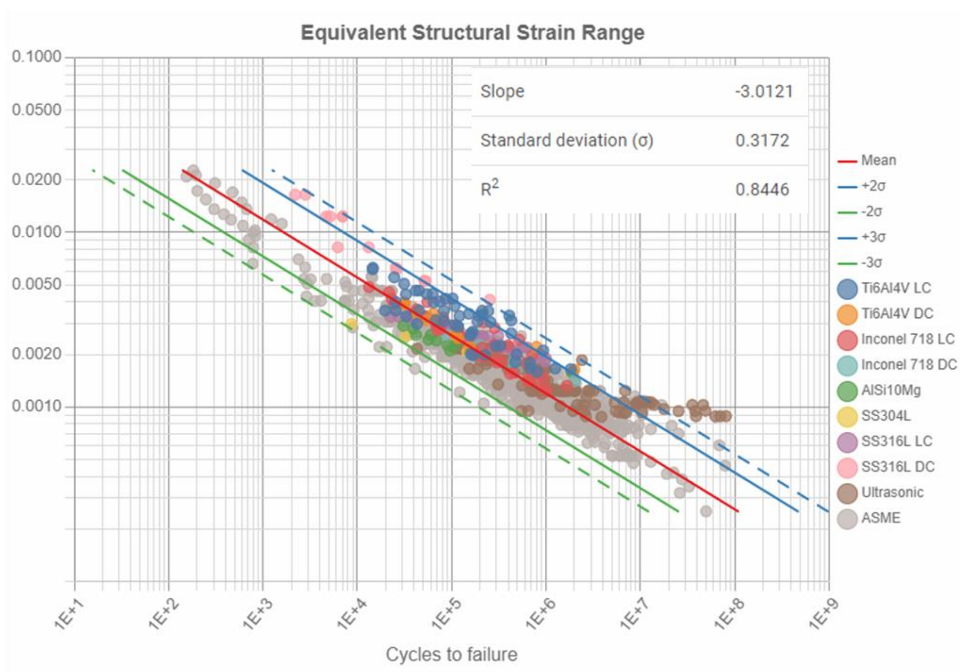

Figure 2-34

It is worth noting that all AM data in Figure 2-33, once plotted together with over 1000 weldment fatigue test data (labeled as “ASME”) show a good correlation (see Figure 2-34) except a few AM data points (ultrasonic tests) situated above the ASME $+3\sigma$ line in the high cycle fatigue regime.

To further examine how the equivalent structural strain parameter given in Eq. (2.5) proves to be an effective parameter in correlating the AM test data. A subset of test data given in Figure 2-33 are considered here for clarity. This subset includes all Ti-6-4, Inconel 718, SS 304, SS316, and aluminum alloy (AlSi10Mg). Four parameter definitions are considered here, i.e., nominal strain range $\Delta\varepsilon_n = \Delta\sigma_n / E$ (Figure 2-35a), structural strain range $\Delta\varepsilon_s = \Delta\sigma_s / E$ (see Figure 2-35b), structural strain range with the thickness correction (*TC*) $\Delta\varepsilon'_s = \Delta\varepsilon_s / t^{(2-m)/2m}$ (see Figure 2-35c), and the equivalent structural strain range $\Delta\mathrm{E}_s = \Delta\varepsilon_s / \left[t^{(2-m)/2m} I(r)^{1/m}\right]$ (see Figure 2-35d) given in Eq. (2.5). As can be seen in Figure 2-35, the data correlation becomes increasingly improved from Figure 2-35a to Figure 2-35d.

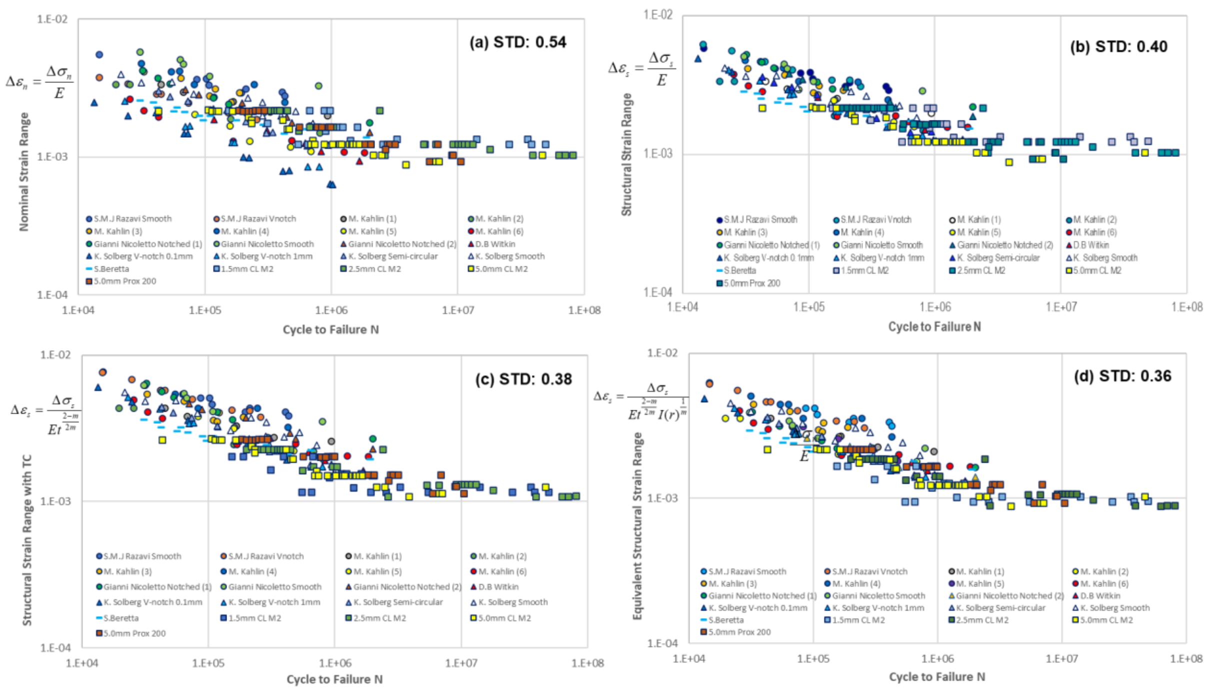

Figure 2-35

2.5 Fitness-for-Service Based Flaw Acceptance Criteria

<u>2.5.1 Problem Definition</u>

To quantitatively evaluate a critical location based flaw acceptance criterion, fracture mechanics based fitness-for-service (FFS) assessment methodology based on API 579-RP (2016) is adopted here. Consider an additively manufactured self-reinforced nozzle component similar to the one shown in Figure 2-19. Specific material and dimensions considered here are given in Figure 2-36. Based on ASME Code, the design pressure based on ASME Code is at 1.7MPa. The fracture toughness in terms of K_{mat} for stainless steel 304L under wrought conditions is given at $132 MPa\sqrt{m}$ by API 579 RP. Due to the lack of fracture toughness test data under AM conditions, a knock-down factor of 0.75 is applied in this assessment.

2.5.2 Stress State Determination

The structural stress results are summarized in Figure 2-37 under 1MPa internal pressure with the end effects (i.e., $Pr/2t$) being considered for the main vessel and nozzle, respectively. Consistent with the results shown in Figure 2-23, the most critical location occurs at the crown position along the circumferential A-A section. Note that the thoroughness bending stress is defined as being positive if OD surface is subjected to tension. As shown in Figure 2-37, the through-thickness bending stress is negative along the entire circumferential section (A-A). This means the ID is subject to positive bending stress. The resulting membrane plus bending with respect to ID surface is given as the orange color line.

For comparison purpose, three positions are considered for further FFS assessment. They are: crown position (A1) and saddle position (A2) along the circumferential section A-A, and a remote reference position (R) on the nozzle, as indicated in Figure 2-37. Note that at Position R, both hoop and axial stresses, attain their nominal values corresponding to Pr/t and $Pr/2t$, respectively, as illustrated in Figure 2-18. The structural stress states corresponding to the design pressure of 1.7MPa at the three positions are also given in Figure 2-37.

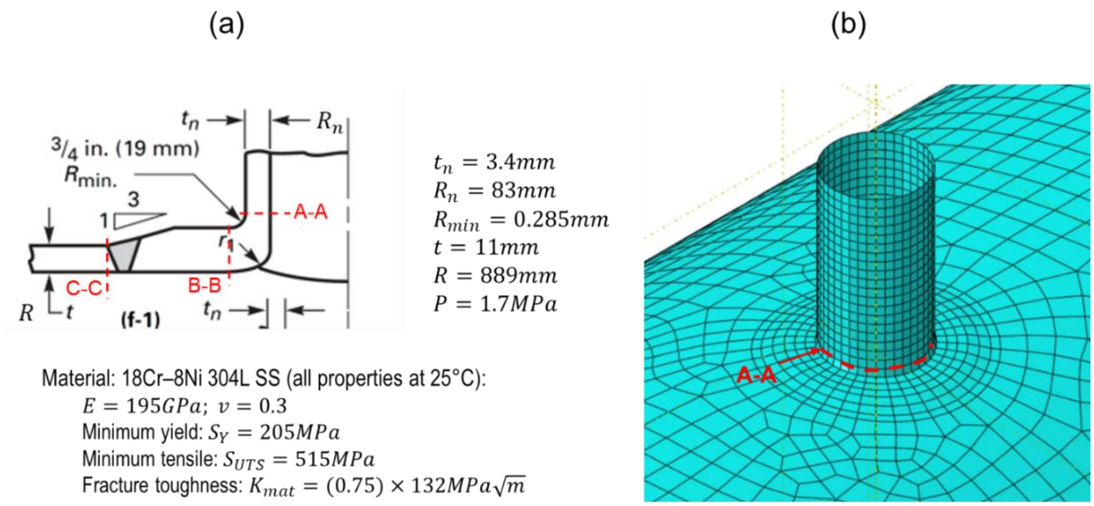

Figure 2-36

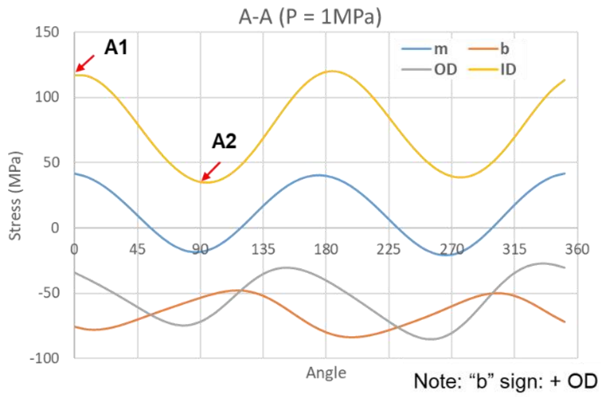

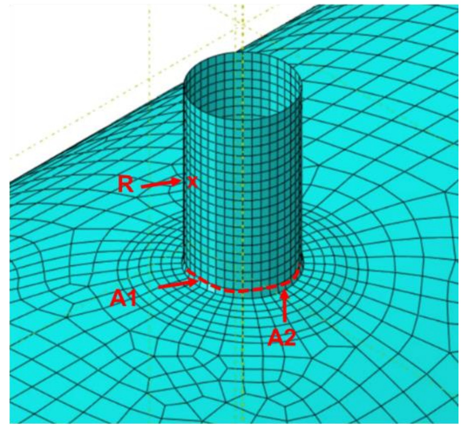

P = 1.7MPa

A-A	Pm, MPa	Pb, MPa
Crown(ID) A1	67.8	135.7
Saddle(ID) A2	-30.8	90.8
Nozzle Reference R	41.5	0

Figure 2-37

2.5.3 FAD Definition

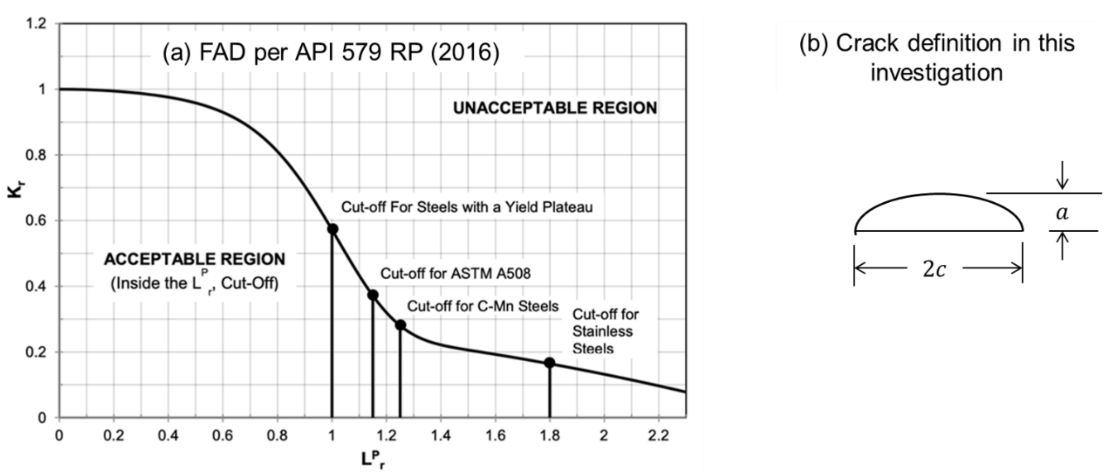

Figure 2-38

According to Part 9.4.3 Level 2 of API 579 RP (2016), the failure assessment diagram (FAD) is given in Figure 2-38a in which $L^P_{r(max)} = 1.8$ is chosen for stainless steels in this investigation. Elliptical crack is considered for at the three positions (see Figure 2-37). At Positions A1 and A2, the elliptical crack plane is perpendicular the nozzle axis direction with the crack length $2c$ being situated on the ID surface with crack depth into the thickness. At Position R, the elliptical crack plane (with $2c$ situated on the ID surface)is parallel to the nozzle longitudinal axis so that nozzle hoop stress is operative. For all three cases, initial crack size is assumed to be a/t = 0.1 and $a/c = 0.1$.

2.5.4 FFS Assessment Results

Due to the complicated geometry at Section A-A, it is important that the stress intensity factor and reference stress solutions in terms of K_r and L_r obtained using API 579-RP (2016) can be validated by available solutions for similar component geometry, e.g., by British Standard BS 7910 (2013). The results are shown in Figure 2-39. As can be seen, both API 579 and BS 7910 yield rather consistent K_r and L_r as the elliptical crack depth increases.

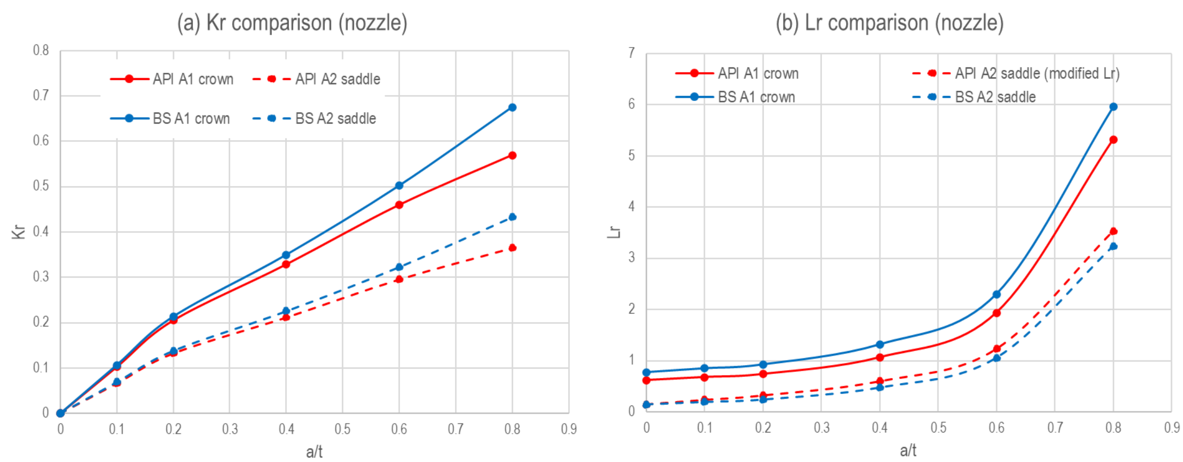

Figure 2-39

By incrementally increasing relative crack depth a/t from its initial value of $a_0/t = 0.1$ and maintaining $a/c = 0.1$, the assessment lines corresponding to the three positions (A1, A2, R) are found intersect at the FAD envelop beyond which unsafe conditions are expected, at the following critical crack sizes:

A1: $\frac{a}{t} < 0.35$

A2: $\frac{a}{t} < 0.61$

R: $\frac{a}{t} < 0.9$

The above critical crack sizes corresponding to the three positions are also summarized graphically in Figure 2-40.

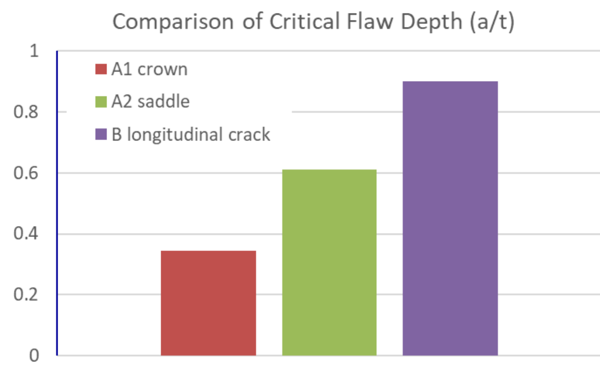

Figure 2-40

The results in Figure 2-40 indicate that Position A1 (crown) can tolerate a much smaller flaw depth due to its high structural stress value. Position A2 (saddle) is capable of tolerating a relatively larger depth, about 40% larger than A2, due to its relatively lower structural stress value. At Position R (about $3\sqrt{rt}$ away from the nozzle and reinforcement pad intersection) can tolerate a flaw depth as much as approximate three times of that at A1.

2.6 Future Fatigue Testing Needs and Test Plan Development

Although a large amount of AM fatigue test data (see Appendix A) has been collected and analyzed in this investigation. The results shown in Figure 2-33 and Figure 2-34 suggest that more data are needed particularly in the low cycle fatigue regime (less than 10^4 cycles to failure) and high cycle fatigue regime (beyond 10^6 cycles to failure) in order to more reliably define fatigue design allowable stress based on the master E-N curve based data representation through Eq. (2.5). Furthermore, for AM component applications, stress gradient effects must be adequately considered in developing such fatigue test data. Based on the insights gained through the data correlation shown in Figure 2-33 and Figure 2-34, two sets of notched fatigue specimens (double edge notched, i.e., DEN; and center notched, i.e., CN) are recommended for consideration, as illustrated in Figure 2-41.

The test conditions and test procedures are recommended as follows:

(1) AM specimens with post-process treatment/AM build orientations of interest (n combinations)

- Double edge notched (DEN) strip specimens
- Center notched (CN) strip specimens

(2) Specimen preparation:

- Individual built with the same scanning conditions at notched root

(3) Test procedure and related requirements

- 3 stress levels with triplicate each (9 + 2 spares)
- Fatigue loading: cyclic tension with R = 0.1
- Load controlled to either complete failure or 50% increase in grip displacement

- Post fracture path examination and documentation, etc.

(4) Total number of specimens needed:

$$N = n \times 2 \times 11$$

The final specimen drawings with final dimensions are given in Appendix B.

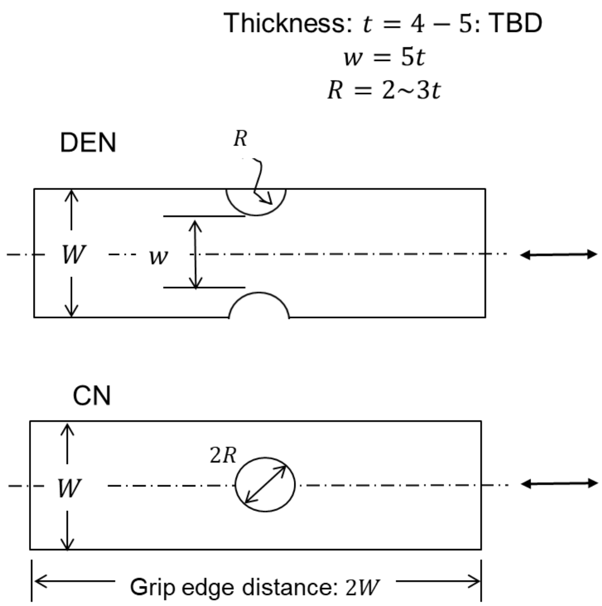

Figure 2-41

3. SUMMARY OF MAJOR FINDINGS

Major findings resulted from this investigation can be summarized as follows:

(1) The master E-N curve based on the master S-N curve and its corresponding scatter band adopted by ASME Section VIII Division 2 Code provides a reasonable fit to the 400 data points evaluated in this project (see Figure 2-30 and Figure 2-33). The somewhat larger scatter band seen in AM specimen test data is largely due to variation in quality definitions and test conditions reported by researchers, often lacking detailed documentations. As for welded components, the master S-N curve scatter band represents weld toe cracking into base metal plate and less affected by weld zone quality characteristics. Post AM thermal and mechanical post-processing does not significantly improve the fatigue life of PBF AM components, particularly in the low cycle fatigue regime (see Figure 2-8, Figure 2-30, and Figure 2-33). In high cycle fatigue regime, post-processing methods seem to show more noticeable effects on PBF AM fatigue behavior.

(2) Recognizing inevitable presence of some level of microscopic geometric discontinuities both at part surface and interior, e.g., lack of fusions, porosities, etc., fatigue test data show that as long as those discontinuities are within a controlled limit with industry's best practice, a consistent fatigue behavior in terms of master S-N curve or E-N curve and its scatter band can be established for extracting fatigue design allowables. The data collected in this investigation supports that as long as the same flaw acceptance is applied, the same deign fatigue curves currently used for welded components can be applied to AM components.

(3) Additional low-cycle fatigue tests incorporating stress gradient effects (e.g., using the proposed notched specimens (DEN and CN) are recommended for improve the master E-N curve representation of the AM test data

(4) A cost-effective AM flaw acceptance criterion can be implemented by identifying fatigue-critical locations in AM components and directing focused NDE at these locations . Current FFS methodologies are shown effective in quantitatively establish flaw acceptance criteria for these hot spot or peak stress locations.

REFERENCES

1. DebRoy, T., et al., *Additive manufacturing of metallic components–process, structure and properties.* Progress in Materials Science, 2018. **92**: p. 112-224.
2. Dong, P., *Quantitative Weld Quality Acceptance Criteria: An Enabler for Structural Lightweighting and Additive Manufacturing* WELDING JOURNAL, 2020. **99**(2): p. 39S-51S.
3. Solberg, K. and F. Berto, *Notch-defect interaction in additively manufactured Inconel 718.* International Journal of Fatigue, 2019. **122**: p. 35-45.
4. Brennan, M., J. Keist, and T. Palmer, *Defects in Metal Additive Manufacturing Processes.* Journal of Materials Engineering and Performance, 2021. **30**(7): p. 4808-4818.
5. Gong, H., et al. *The effects of processing parameters on defect regularity in Ti-6Al-4V parts fabricated by selective laser melting and electron beam melting*. in *24th annual international solid freeform fabrication symposium—an additive manufacturing conference, Austin, TX*. 2013.
6. Zhang, M., et al., *Fatigue and fracture behaviour of laser powder bed fusion stainless steel 316L: Influence of processing parameters.* Materials Science and Engineering: A, 2017. **703**: p. 251-261.
7. Sanaei, N. and A. Fatemi, *Defects in additive manufactured metals and their effect on fatigue performance: A state-of-the-art review.* Progress in Materials Science, 2021. **117**: p. 100724.
8. Zhang, M., et al., *High cycle fatigue and ratcheting interaction of laser powder bed fusion stainless steel 316L: Fracture behaviour and stress-based modelling.* International Journal of Fatigue, 2019. **121**: p. 252-264.
9. Cegan, T., et al., *Effect of Hot Isostatic Pressing on Porosity and Mechanical Properties of 316 L Stainless Steel Prepared by the Selective Laser Melting Method.* Materials, 2020. **13**(19): p. 4377.
10. Ziółkowski, G., et al., *Application of X-ray CT method for discontinuity and porosity detection in 316L stainless steel parts produced with SLM technology.* Archives of civil and mechanical engineering, 2014. **14**(4): p. 608-614.
11. Hatami, S., et al., *Fatigue strength of 316 L stainless steel manufactured by selective laser melting.* Journal of Materials Engineering and Performance, 2020. **29**: p. 3183-3194.

12. Dong, P., et al., *The master SN curve method an implementation for fatigue evaluation of welded components in the ASME B&PV Code, Section VIII, Division 2 and API 579-1/ASME FFS-1.* Welding Research Council Bulletin, 2010(523).
13. Ferrell, R., *Alteration Plan NBIC Part3/ASME Section VIII Div. 1 – Additional of a large nozzle to a pressure vessel*. 2019, NB members meeting 2019.
14. Dong, P., Z. Wei, and J.K. Hong, *A path-dependent cycle counting method for variable-amplitude multi-axial loading.* International Journal of Fatigue, 2010. **32**(4): p. 720-734.
15. Dong, P., et al., *On residual stress prescriptions for fitness for service assessment of pipe girth welds.* International Journal of Pressure Vessels and Piping, 2014. **123**: p. 19-29.
16. Dong, P., J. Hong, and Z. Cao, *Stresses and stress intensities at notches:'anomalous crack growth'revisited.* International journal of fatigue, 2003. **25**(9-11): p. 811-825.
17. Pei, X., P. Dong, and S. Xing, *A structural strain parameter for a unified treatment of fatigue behaviors of welded components.* International Journal of Fatigue, 2019.
18. Brenne, F. and T. Niendorf, *Effect of notches on the deformation behavior and damage evolution of additively manufactured 316L specimens under uniaxial quasi-static and cyclic loading.* International Journal of Fatigue, 2019. **127**: p. 175-189.
19. Smith, T.R., et al., *Relationship between manufacturing defects and fatigue properties of additive manufactured austenitic stainless steel.* Materials Science and Engineering: A, 2019. **765**: p. 138268.
20. Shrestha, R., J. Simsiriwong, and N. Shamsaei, *Fatigue behavior of additive manufactured 316L stainless steel under axial versus rotating-bending loading: Synergistic effects of stress gradient, surface roughness, and volumetric defects.* International Journal of Fatigue, 2021. **144**: p. 106063.
21. Tate, D.G.a., *EPRI Report: ICME and In-Situ Process Monitoring for Rapid Qualification of Components Made by Laser-based Powder Bed Additive Manufacturing Processes for Nuclear Structural Applications*. 2020, EPRI.
22. Shrestha, R., J. Simsiriwong, and N. Shamsaei, *Fatigue behavior of additive manufactured 316L stainless steel parts: Effects of layer orientation and surface roughness.* Additive Manufacturing, 2019. **28**: p. 23-38.

APPENDIX A: AM FATIGUE TEST DATA ANALYZED

Terminologies used in fatigue test data documentation

N	Number of Cycles to Failure
Max Stress	Maximum or Peak Nominal Stress Reported
Te	Expected Final Depth at the end of Test
TC	Thickness Correction Term Per Equivalent Structural Stress Definition
SCFm	Membrane SCF calculated wrt nominal stress
SCFb	Bending SCF calculated wrt nominal stress
R	Load Ratio
SS range	Structural Stress Range
SE range	Structural Strain Range
SE TC	Structural Strain Range with Thickness Correction
r	Bending Ratio: SCFb/SCF
I(r)	Loading Mode Correction Term
ESE Range	Equivalent Structural Strain Range
S Range	Nominal Stress Range

1 **S.M.J Razavi Smooth** https://www.sciencedirect.com/science/article/pii/S0167844217302884

AM Process	Post AM Treatment	Material Type	Specimen Geometry	LC/DC	Loading Type	Failure Criterion	N	Max Stress	Te	TC	SCFm	SCFb	SCF	R	SS Range	E/1000000	SE Range	SE TC	r	I(r)^(1/m	ESE Rang	Srange
SLM	Sandblast, stress relief heat treatment 650C for 3h	Ti6Al4V	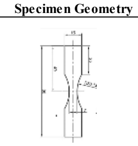	LC	Tension	Separation	14639	589.621668	3.5	0.757	1	0.052837	1.052837	0	620.7755	110000	0.005643	0.007455	0.050185	1.22307	0.006095	589.6217
							86527.78	392.21965	3.5	0.757	1	0.052837	1.052837	0	412.9434	110000	0.003754	0.004959	0.050185	1.22307	0.004055	392.2197
							102601	393.759768	3.5	0.757	1	0.052837	1.052837	0	414.5649	110000	0.003769	0.004979	0.050185	1.22307	0.004071	393.7598
							107603	355.73074	3.5	0.757	1	0.052837	1.052837	0	374.5265	110000	0.003405	0.004498	0.050185	1.22307	0.003677	355.7307
							195066	313.487229	3.5	0.757	1	0.052837	1.052837	0	330.051	110000	0.003	0.003964	0.050185	1.22307	0.003241	313.4872
							211517	334.508795	3.5	0.757	1	0.052837	1.052837	0	352.1832	110000	0.003202	0.004229	0.050185	1.22307	0.003458	334.5088
							409140	314.557356	3.5	0.757	1	0.052837	1.052837	0	331.1776	110000	0.003011	0.003977	0.050185	1.22307	0.003252	314.5574
							429193	294.756116	3.5	0.757	1	0.052837	1.052837	0	310.3301	110000	0.002821	0.003727	0.050185	1.22307	0.003047	294.7561

2 **S.M.J Razavi Vnotch** https://www.sciencedirect.com/science/article/pii/S0167844217302884

AM Process	Post AM Treatment	Material Type	Specimen Geometry	LC/DC	Loading Type	Failure Criterion	N	Max Stress	Te	TC	SCFm	SCFb	SCF	R	SS Range	E/1000000	SE Range	SE TC	r	I(r)^(1/m	ESE Rang	Srange
SLM	Sandblast, stress relief heat treatment 650C for 3h	Ti6Al4V	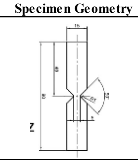	LC	Tension	Separation	14581.09	403.004351	2.5	0.815772	1	0.644151	1.644151	0	662.6	110000	0.006024	0.007384	0.391783	1.23525	0.005978	403.0044
							24640.54	362.486666	2.5	0.815772	1	0.644151	1.644151	0	595.9828	110000	0.005418	0.006642	0.391783	1.23525	0.005377	362.4867
							41660.17	304.218654	2.5	0.815772	1	0.644151	1.644151	0	500.1814	110000	0.004547	0.005574	0.391783	1.23525	0.004512	304.2187
							45157.18	304.218654	2.5	0.815772	1	0.644151	1.644151	0	500.1814	110000	0.004547	0.005574	0.391783	1.23525	0.004512	304.2187
							74506.93	263.778223	2.5	0.815772	1	0.644151	1.644151	0	433.6912	110000	0.003943	0.004833	0.391783	1.23525	0.003913	263.7782
							152842.6	224.100321	2.5	0.815772	1	0.644151	1.644151	0	368.4548	110000	0.00335	0.004106	0.391783	1.23525	0.003324	224.1003
							212712.5	222.28116	2.5	0.815772	1	0.644151	1.644151	0	365.4638	110000	0.003322	0.004073	0.391783	1.23525	0.003297	222.2812
							258295.5	200.749683	2.5	0.815772	1	0.644151	1.644151	0	330.0628	110000	0.003001	0.003678	0.391783	1.23525	0.002978	200.7497

3 **M. Kahlin (1)** https://www.sciencedirect.com/science/article/pii/S0142112317301809

AM Process	Post AM Treatment	Material Type	Specimen Geometry	LC/DC	Loading Type	Failure Criterion	N	Max Stress	Te	TC	SCFm	SCFb	SCF	R	SS Range	E/1000000	SE Range	SE TC	r	I(r)^(1/m	ESE Rang	Srange
EBM	Blasted with Titanium powder, HIP	Ti6Al4V	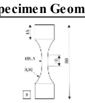	LC	Tension	Separation	45309.76	398.668895	3.25	0.76957	1	0	1	0.1	358.802	114000	0.003147	0.00409	0	1.2223	0.003346	358.802
							67924.11	349.832247	3.25	0.76957	1	0	1	0.1	314.849	114000	0.002762	0.003589	0	1.2223	0.002936	314.849
							167312.3	299.888511	3.25	0.76957	1	0	1	0.1	269.8997	114000	0.002368	0.003076	0	1.2223	0.002517	269.8997
							328857.6	251.098643	3.25	0.76957	1	0	1	0.1	225.9888	114000	0.001982	0.002576	0	1.2223	0.002107	225.9888
							936935	235.77248	3.25	0.76957	1	0	1	0.1	212.1952	114000	0.001861	0.002419	0	1.2223	0.001979	212.1952

4 **M. Kahlin (2)** https://www.sciencedirect.com/science/article/pii/S0142112317301809

AM Process	Post AM Treatment	Material Type	Specimen Geometry	LC/DC	Loading Type	Failure Criterion	N	Max Stress	Te	TC	SCFm	SCFb	SCF	R	SS Range	E/1000000	SE Range	SE TC	r	I(r)^(1/m	ESE Rang	Srange
EBM	Blasted with Titanium powder	Ti6Al4V	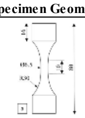	LC	Tension	Separation	19742.66	398.525441	3.25	0.76957	1	0	1	0.1	358.6729	114000	0.003146	0.004088	0	1.2223	0.003345	358.6729
							25652.62	398.57066	3.25	0.76957	1	0	1	0.1	358.7136	114000	0.003147	0.004089	0	1.2223	0.003345	358.7136
							159565	224.731219	3.25	0.76957	1	0	1	0.1	202.2581	114000	0.001774	0.002305	0	1.2223	0.001886	202.2581
							292423	249.885523	3.25	0.76957	1	0	1	0.1	224.897	114000	0.001973	0.002563	0	1.2223	0.002097	224.897
							676183.4	199.930872	3.25	0.76957	1	0	1	0.1	179.9378	114000	0.001578	0.002051	0	1.2223	0.001678	179.9378
							809468.6	177.297924	3.25	0.76957	1	0	1	0.1	159.5681	114000	0.0014	0.001819	0	1.2223	0.001488	159.5681

5 **M. Kahlin (3)** https://www.sciencedirect.com/science/article/pii/S0142112317301809

AM Process	Post AM Treatment	Material Type	Specimen Geometry	LC/DC	Loading Type	Failure Criterion	N	Max Stress	Te	TC	SCFm	SCFb	SCF	R	SS Range	E/1000000	SE Range	SE TC	r	I(r)^(1/m)	ESE Range	Srange
LS	stress relieved at 650C for 3h and sandblasted, HIP	Ti6Al4V	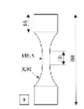	LC	Tension	Separation	32829.33	494.040692	3.25	0.76957	1	0	1	0.1	444.6366	114000	0.0039	0.005068	0	1.2223	0.004146	444.6366
							64524.74	444.057974	3.25	0.76957	1	0	1	0.1	399.6522	114000	0.003506	0.004555	0	1.2223	0.003727	399.6522
							121139.7	371.403326	3.25	0.76957	1	0	1	0.1	334.263	114000	0.002932	0.00381	0	1.2223	0.003117	334.263
							109547.7	329.636454	3.25	0.76957	1	0	1	0.1	296.6728	114000	0.002602	0.003382	0	1.2223	0.002767	296.6728
							117724.5	321.298984	3.25	0.76957	1	0	1	0.1	289.1691	114000	0.002537	0.003296	0	1.2223	0.002697	289.1691
							188408.8	345.23705	3.25	0.76957	1	0	1	0.1	310.7133	114000	0.002726	0.003542	0	1.2223	0.002898	310.7133
							161353.8	295.110878	3.25	0.76957	1	0	1	0.1	265.5998	114000	0.00233	0.003027	0	1.2223	0.002477	265.5998

6 **M. Kahlin (4)** https://www.sciencedirect.com/science/article/pii/S0142112317301809

AM Process	Post AM Treatment	Material Type	Specimen Geometry	LC/DC	Loading Type	Failure Criterion	N	Max Stress	Te	TC	SCFm	SCFb	SCF	R	SS Range	E/1000000	SE Range	SE TC	r	I(r)^(1/m)	ESE Range	Srange
LS	stress relieved at 650C for 3h and sandblasted	Ti6Al4V	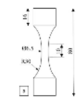	LC	Tension	Separation	31450.01	567.989542	3.25	0.76957	1	0	1	0.1	511.1906	114000	0.004484	0.005827	0	1.2223	0.004767	511.1906
							54436.05	495.320861	3.25	0.76957	1	0	1	0.1	445.7888	114000	0.00391	0.005081	0	1.2223	0.004157	445.7888
							62899.56	496.538658	3.25	0.76957	1	0	1	0.1	446.8848	114000	0.00392	0.005094	0	1.2223	0.004167	446.8848
							82970.3	397.580517	3.25	0.76957	1	0	1	0.1	357.8225	114000	0.003139	0.004079	0	1.2223	0.003337	357.8225
							245187.2	396.574782	3.25	0.76957	1	0	1	0.1	356.9173	114000	0.003131	0.004068	0	1.2223	0.003328	356.9173
							427869	295.27928	3.25	0.76957	1	0	1	0.1	265.7514	114000	0.002331	0.003029	0	1.2223	0.002478	265.7514

7 **M. Kahlin (5)** https://www.sciencedirect.com/science/article/pii/S0142112317301809

AM Process	Post AM Treatment	Material Type	Specimen Geometry	LC/DC	Loading Type	Failure Criterion	N	Max Stress	Te	TC	SCFm	SCFb	SCF	R	SS Range	E/1000000	SE Range	SE TC	r	I(r)^(1/m)	ESE Range	Srange
EBM	Blasted with Titanium powder, HIP	Ti6Al4V	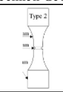	LC	Tension	Separation	83187.66	241.050982	3.25	0.76957	1	0.448484	1.448484	0.1	314.2426	114000	0.002757	0.003582	0.309623	1.230873	0.00291	216.9459
							158284.6	199.855178	3.25	0.76957	1	0.448484	1.448484	0.1	260.5383	114000	0.002285	0.00297	0.309623	1.230873	0.002413	179.8697
							226013.3	154.173942	3.25	0.76957	1	0.448484	1.448484	0.1	200.9866	114000	0.001763	0.002291	0.309623	1.230873	0.001861	138.7565
							474159.5	140.586917	3.25	0.76957	1	0.448484	1.448484	0.1	183.2741	114000	0.001608	0.002089	0.309623	1.230873	0.001697	126.5282
							686841.8	129.848148	3.25	0.76957	1	0.448484	1.448484	0.1	169.2747	114000	0.001485	0.001929	0.309623	1.230873	0.001568	116.8633

8 **M. Kahlin (6)** https://www.sciencedirect.com/science/article/pii/S0142112317301809

AM Process	Post AM Treatment	Material Type	Specimen Geometry	LC/DC	Loading Type	Failure Criterion	N	Max Stress	Te	TC	SCFm	SCFb	SCF	R	SS Range	E/1000000	SE Range	SE TC	r	I(r)^(1/m)	ESE Range	Srange
EBM	Blasted with Titaniium powder	Ti6Al4V	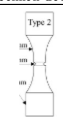	LC	Tension	Separation	25548.63	311.034579	3.25	0.76957	1	0.448484	1.448484	0.1	405.4758	114000	0.003557	0.004622	0.309623	1.230873	0.003755	279.9311
							33072.92	256.907238	3.25	0.76957	1	0.448484	1.448484	0.1	334.9134	114000	0.002938	0.003818	0.309623	1.230873	0.003101	231.2165
							43110.17	232.650508	3.25	0.76957	1	0.448484	1.448484	0.1	303.2915	114000	0.00266	0.003457	0.309623	1.230873	0.002809	209.3855
							168315.9	154.19799	3.25	0.76957	1	0.448484	1.448484	0.1	201.018	114000	0.001763	0.002291	0.309623	1.230873	0.001862	138.7782
							488552.1	155.801869	3.25	0.76957	1	0.448484	1.448484	0.1	203.1089	114000	0.001782	0.002315	0.309623	1.230873	0.001881	140.2217
							1257316	129.235209	3.25	0.76957	1	0.448484	1.448484	0.1	168.4756	114000	0.001478	0.00192	0.309623	1.230873	0.00156	116.3117
							1834717	128.077161	3.25	0.76957	1	0.448484	1.448484	0.1	166.9659	114000	0.001465	0.001903	0.309623	1.230873	0.001546	115.2694

9 **Gianni Nicoletto Notched (1)** https://www.sciencedirect.com/science/article/pii/S0142112317303961

AM Process	Post AM Treatment	Material Type	Specimen Geometry	LC/DC	Loading Type	Failure Criterion	N	Max Stress	Te	TC	SCFm	SCFb	SCF	R	SS Range	E/1000000	SE Range	SE TC	r	I(r)^(1/m)	ESE Range	Srange
SLM	Heat Treated	Ti6Al4V		DC	Bending	Initiation	32213.55	453.800298	2.5	0.815772	0.47189	0.762495	1.234385	0	560.1643	114000	0.004914	0.006023	0.617712	1.640019	0.003673	453.8003
							42680.07	398.509687	2.5	0.815772	0.47189	0.762495	1.234385	0	491.9144	114000	0.004315	0.00529	0.617712	1.640019	0.003225	398.5097
							53295.2	364.083458	2.5	0.815772	0.47189	0.762495	1.234385	0	449.4192	114000	0.003942	0.004833	0.617712	1.640019	0.002947	364.0835
							116821.9	287.928465	2.5	0.815772	0.47189	0.762495	1.234385	0	355.4146	114000	0.003118	0.003822	0.617712	1.640019	0.00233	287.9285
							154778.5	256.631893	2.5	0.815772	0.47189	0.762495	1.234385	0	316.7826	114000	0.002779	0.003406	0.617712	1.640019	0.002077	256.6319
							2005630	189.865872	2.5	0.815772	0.47189	0.762495	1.234385	0	234.3676	114000	0.002056	0.00252	0.617712	1.640019	0.001537	189.8659

10 **Gianni Nicoletto Smooth** https://www.sciencedirect.com/science/article/pii/S0142112317303961

AM Process	Post AM Treatment	Material Type	Specimen Geometry	LC/DC	Loading Type	Failure Criterion	N	Max Stress	Te	TC	SCFm	SCFb	SCF	R	SS Range	E/1000000	SE Range	SE TC	r	I(r)^(1/m)	ESE Range	Srange
SLM	Heat Treated	Ti6Al4V		DC	Bending	Initiation	30813.85	616.542474	2.5	0.815772	0.471775	0.40619	0.877965	0	541.3027	114000	0.004748	0.005821	0.462649	1.596416	0.003646	616.5425
							64131.88	543.517139	2.5	0.815772	0.47189	0.40619	0.87808	0	477.2515	114000	0.004186	0.005132	0.462589	1.596403	0.003215	543.5171
							67543.26	504.918033	2.5	0.815772	0.47189	0.40619	0.87808	0	443.3584	114000	0.003889	0.004767	0.462589	1.596403	0.002986	504.918
							108485	411.028316	2.5	0.815772	0.47189	0.40619	0.87808	0	360.9157	114000	0.003166	0.003881	0.462589	1.596403	0.002431	411.0283
							794916.6	350.52161	2.5	0.815772	0.47189	0.40619	0.87808	0	307.786	114000	0.0027	0.00331	0.462589	1.596403	0.002073	350.5216

11 **Gianni Nicoletto Notched (2)** https://www.sciencedirect.com/science/article/pii/S0142112319303019

AM Process	Post AM Treatment	Material Type	Specimen Geometry	LC/DC	Loading Type	Failure Criterion	N	Max Stress	Te	TC	SCFm	SCFb	SCF	R	SS Range	E/1000000	SE Range	SE TC	r	I(r)^(1/m)	ESE Range	Srange
SLM	Heat Treated	Inconel 718		DC	Bending	Initiation	70396.25	612.102874	2.5	0.815772	0.47189	0.762495	1.234385	0	755.5706	200000	0.003778	0.004631	0.617712	1.640019	0.002824	612.1029
							89344.14	560.2118	2.5	0.815772	0.47189	0.762495	1.234385	0	691.517	200000	0.003458	0.004238	0.617712	1.640019	0.002584	560.2118
							197384.2	490.3177	2.5	0.815772	0.47189	0.762495	1.234385	0	605.2408	200000	0.003026	0.00371	0.617712	1.640019	0.002262	490.3177
							442823.2	386.535552	2.5	0.815772	0.47189	0.762495	1.234385	0	477.1337	200000	0.002386	0.002924	0.617712	1.640019	0.001783	386.5356
							488509.9	352.647504	2.5	0.815772	0.47189	0.762495	1.234385	0	435.3028	200000	0.002177	0.002668	0.617712	1.640019	0.001627	352.6475
							2010008	301.815431	2.5	0.815772	0.47189	0.762495	1.234385	0	372.5564	200000	0.001863	0.002283	0.617712	1.640019	0.001392	301.8154

12 **D.B Witkin**

AM Process	Post AM Treatment	Material Type	Specimen Geometry	LC/DC	Loading Type	Failure Criterion	N	Max Stress	Te	TC	SCFm	SCFb	SCF	R	SS Range	E/1000000	SE Range	SE TC	r	I(r)^(1/m)	ESE Range	Srange
SLM	Heat Treated, HIP	Inconel 718		LC	Tension	Initiation	118328.1	414.060414	2.825	0.793914	1.191213	0.18481	1.376023	0.1	512.781	200000	0.002564	0.003229	0.134307	1.224779	0.002637	372.6544
							308511.1	346.209593	2.825	0.793914	1.191213	0.18481	1.376023	0.1	428.7531	200000	0.002144	0.0027	0.134307	1.224779	0.002205	311.5886
							618617.8	277.465397	2.825	0.793914	1.191213	0.18481	1.376023	0.1	343.6189	200000	0.001718	0.002164	0.134307	1.224779	0.001767	249.7189
							833430.4	242.666198	2.825	0.793914	1.191213	0.18481	1.376023	0.1	300.5228	200000	0.001503	0.001893	0.134307	1.224779	0.001545	218.3996
							1672260	206.302231	2.825	0.793914	1.191213	0.18481	1.376023	0.1	255.489	200000	0.001277	0.001609	0.134307	1.224779	0.001314	185.672

13 **K. Solberg V-notch 0.1mm** https://www.sciencedirect.com/science/article/pii/S0142112318307382

AM Process	Post AM Treatment	Material Type	Specimen Geometry	LC/DC	Loading Type	Failure Criterion	N	Max Stress	Te	TC	SCFm	SCFb	SCF	R	SS Range	E/1000000	SE Range	SE TC	r	I(r)^(1/m	ESE Rang	Srange
SLM		Inconel 718	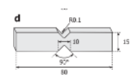	LC	Tension	Separation	13315.17	493.488812	2.5	0.815772	1.145669	0.83283	1.978499	0	976.3673	208000	0.004694	0.005754	0.42094	1.237083	0.004651	493.4888
							24644.71	395.037801	2.5	0.815772	1.145669	0.83283	1.978499	0	781.582	208000	0.003758	0.004606	0.42094	1.237083	0.003723	395.0378
							68800.69	295.520924	2.5	0.815772	1.145669	0.83283	1.978499	0	584.688	208000	0.002811	0.003446	0.42094	1.237083	0.002785	295.5209
							73291.79	292.675625	2.5	0.815772	1.145669	0.83283	1.978499	0	579.0585	208000	0.002784	0.003413	0.42094	1.237083	0.002759	292.6756
							201262.4	198.755579	2.5	0.815772	1.145669	0.83283	1.978499	0	393.2378	208000	0.001891	0.002318	0.42094	1.237083	0.001873	198.7556
							224824.6	196.841945	2.5	0.815772	1.145669	0.83283	1.978499	0	389.4517	208000	0.001872	0.002295	0.42094	1.237083	0.001855	196.8419
							416122.2	157.57198	2.5	0.815772	1.145669	0.83283	1.978499	0	311.7561	208000	0.001499	0.001837	0.42094	1.237083	0.001485	157.572
							464900.2	159.103844	2.5	0.815772	1.145669	0.83283	1.978499	0	314.7869	208000	0.001513	0.001855	0.42094	1.237083	0.0015	159.1038
							976606.5	127.362629	2.5	0.815772	1.145669	0.83283	1.978499	0	251.9869	208000	0.001211	0.001485	0.42094	1.237083	0.0012	127.3626
							1024022	126.136372	2.5	0.815772	1.145669	0.83283	1.978499	0	249.5607	208000	0.0012	0.001471	0.42094	1.237083	0.001189	126.1364

14 **K. Solberg V-notch 1mm** https://www.sciencedirect.com/science/article/pii/S0142112318307382

AM Process	Post AM Treatment	Material Type	Specimen Geometry	LC/DC	Loading Type	Failure Criterion	N	Max Stress	Te	TC	SCFm	SCFb	SCF	R	SS Range	E/1000000	SE Range	SE TC	r	I(r)^(1/m	ESE Rang	Srange
SLM		Inconel 718	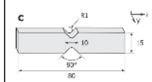	LC	Tension	Separation	23201.56	503.130531	2.5	0.815772	1	0.610368	1.610368	0	810.2254	208000	0.003895	0.004775	0.37902	1.234496	0.003868	503.1305
							41095.39	418.647729	2.5	0.815772	1	0.610368	1.610368	0	674.177	208000	0.003241	0.003973	0.37902	1.234496	0.003218	418.6477
							70514.08	331.90088	2.5	0.815772	1	0.610368	1.610368	0	534.4826	208000	0.00257	0.00315	0.37902	1.234496	0.002552	331.9009
							76341.14	335.127513	2.5	0.815772	1	0.610368	1.610368	0	539.6787	208000	0.002595	0.003181	0.37902	1.234496	0.002576	335.1275
							163603.7	253.140332	2.5	0.815772	1	0.610368	1.610368	0	407.6491	208000	0.00196	0.002402	0.37902	1.234496	0.001946	253.1403
							171586.4	253.140332	2.5	0.815772	1	0.610368	1.610368	0	407.6491	208000	0.00196	0.002402	0.37902	1.234496	0.001946	253.1403
							651318	168.612884	2.5	0.815772	1	0.610368	1.610368	0	271.5288	208000	0.001305	0.0016	0.37902	1.234496	0.001296	168.6129
							800660.3	168.612884	2.5	0.815772	1	0.610368	1.610368	0	271.5288	208000	0.001305	0.0016	0.37902	1.234496	0.001296	168.6129

15 **K. Solberg Semi-circular** https://www.sciencedirect.com/science/article/pii/S0142112318307382

AM Process	Post AM Treatment	Material Type	Specimen Geometry	LC/DC	Loading Type	Failure Criterion	N	Max Stress	Te	TC	SCFm	SCFb	SCF	R	SS Range	E/1000000	SE Range	SE TC	r	I(r)^(1/m	ESE Rang	Srange
SLM		Inconel 718	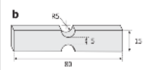	LC	Tension	Separation	42971.7	601.014828	2.5	0.815772	1.000884	0.200286	1.20117	0	721.9209	208000	0.003471	0.004255	0.166742	1.225621	0.003471	601.0148
							52860.34	545.131567	2.5	0.815772	1.000884	0.200286	1.20117	0	654.7956	208001	0.003148	0.003859	0.166742	1.225621	0.003149	545.1316
							73823.13	504.011004	2.5	0.815772	1.000884	0.200286	1.20117	0	605.4028	208002	0.002911	0.003568	0.166742	1.225621	0.002911	504.011
							117104.5	443.777166	2.5	0.815772	1.000884	0.200286	1.20117	0	533.0517	208003	0.002563	0.003141	0.166742	1.225621	0.002563	443.7772
							211038.1	361.424611	2.5	0.815772	1.000884	0.200286	1.20117	0	434.1323	208004	0.002087	0.002558	0.166742	1.225621	0.002087	361.4246
							304485	297.367609	2.5	0.815772	1.000884	0.200286	1.20117	0	357.189	208005	0.001717	0.002105	0.166742	1.225621	0.001718	297.3676
							345708.5	300.190353	2.5	0.815772	1.000884	0.200286	1.20117	0	360.5796	208006	0.001734	0.002125	0.166742	1.225621	0.001734	300.1904
							643204	239.762612	2.5	0.815772	1.000884	0.200286	1.20117	0	287.9956	208007	0.001385	0.001697	0.166742	1.225621	0.001385	239.7626
							941541.1	241.908837	2.5	0.815772	1.000884	0.200286	1.20117	0	290.5736	208008	0.001397	0.001712	0.166742	1.225621	0.001397	241.9088

16 **K. Solberg Smooth** https://www.sciencedirect.com/science/article/pii/S0142112318307382

AM Process	Post AM Treatment	Material Type	Specimen Geometry	LC/DC	Loading Type	Failure Criterion	N	Max Stress	Te	TC	SCFm	SCFb	SCF	R	SS Range	E/1000000	SE Range	SE TC	r	I(r)^(1/m	ESE Rang	Srange
SLM		Inconel 718	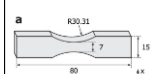	LC	Tension	Separation	21698	794.328235	3.5	0.757	0.997083	0.0569	1.053983	0	837.2082	208000	0.004025	0.005317	0.053986	1.223134	0.004347	794.3282
							31619.91	691.830971	3.5	0.757	0.997083	0.0569	1.053983	0	729.1779	208000	0.003506	0.004631	0.053986	1.223134	0.003786	691.831
							55285.32	698.232404	3.5	0.757	0.997083	0.0569	1.053983	0	735.9249	208000	0.003538	0.004674	0.053986	1.223134	0.003821	698.2324
							81756.93	570.164272	3.5	0.757	0.997083	0.0569	1.053983	0	600.9433	208000	0.002889	0.003817	0.053986	1.223134	0.00312	570.1643
							149299.7	436.515832	3.5	0.757	0.997083	0.0569	1.053983	0	460.0802	208000	0.002212	0.002922	0.053986	1.223134	0.002389	436.5158
							218057.2	534.564359	3.5	0.757	0.997083	0.0569	1.053983	0	563.4216	208000	0.002709	0.003578	0.053986	1.223134	0.002925	534.5644
							286018.1	496.592321	3.5	0.757	0.997083	0.0569	1.053983	0	523.3997	208000	0.002516	0.003324	0.053986	1.223134	0.002718	496.5923
							285603.8	398.107171	3.5	0.757	0.997083	0.0569	1.053983	0	419.5981	208000	0.002017	0.002665	0.053986	1.223134	0.002179	398.1072
							303109.8	346.73685	3.5	0.757	0.997083	0.0569	1.053983	0	365.4547	208000	0.001757	0.002321	0.053986	1.223134	0.001898	346.7369
							398107.2	394.457302	3.5	0.757	0.997083	0.0569	1.053983	0	415.7512	208000	0.001999	0.00264	0.053986	1.223134	0.002159	394.4573
							522688.1	424.619564	3.5	0.757	0.997083	0.0569	1.053983	0	447.5417	208000	0.002152	0.002842	0.053986	1.223134	0.002324	424.6196
							716754.6	346.73685	3.5	0.757	0.997083	0.0569	1.053983	0	365.4547	208000	0.001757	0.002321	0.053986	1.223134	0.001898	346.7369

17 **Thale R.Smith CNT_T(low)** https://www.sciencedirect.com/science/article/pii/S0921509319310548

AM Process	Post AM Treatment	Material Type	Specimen Geometry	LC/DC	Loading Type	Failure Criterion	N	Max Stress	Te	TC	SCFm	SCFb	SCF	R	SS Range	E/1000000	SE Range	SE TC	r	I(r)^(1/m	ESE Rang	Srange
DED		SS304L		LC	Tension	Separation	3542.385	443.094933	2	0.857244	1	0.541379	1.541379	0.1	614.6795	204000	0.003013	0.003515	0.35123	1.232951	0.002851	398.7854
							17639.2	375.864277	2	0.857244	1	0.541379	1.541379	0.1	521.4144	204000	0.002556	0.002982	0.35123	1.232951	0.002418	338.2778
							35538.92	305.866106	2	0.857244	1	0.541379	1.541379	0.1	424.31	204000	0.00208	0.002426	0.35123	1.232951	0.001968	275.2795
							68869.7	305.994147	2	0.857244	1	0.541379	1.541379	0.1	424.4877	204000	0.002081	0.002427	0.35123	1.232951	0.001969	275.3947

18 **Thale R.Smith CNT_L(High)** https://www.sciencedirect.com/science/article/pii/S0921509319310548

AM Process	Post AM Treatment	Material Type	Specimen Geometry	LC/DC	Loading Type	Failure Criterion	N	Max Stress	Te	TC	SCFm	SCFb	SCF	R	SS Range	E/1000000	SE Range	SE TC	r	I(r)^(1/m	ESE Rang	Srange
DED		SS304L		LC	Tension	Separation	8670.181	444.561917	2	0.857244	1	0.541379	1.541379	0.1	616.7146	204000	0.003023	0.003527	0.35123	1.232951	0.00286	400.1057
							32559.37	377.278215	2	0.857244	1	0.541379	1.541379	0.1	523.3758	204000	0.002566	0.002993	0.35123	1.232951	0.002427	339.5504
							147097.6	307.431864	2	0.857244	1	0.541379	1.541379	0.1	426.4821	204000	0.002091	0.002439	0.35123	1.232951	0.001978	276.6887
							166930.3	307.455643	2	0.857244	1	0.541379	1.541379	0.1	426.5151	204000	0.002091	0.002439	0.35123	1.232951	0.001978	276.7101

19 **S.Beretta** https://www.sciencedirect.com/science/article/pii/S0142112320302681

AM Process	Post AM Treatment	Material Type	Specimen Geometry	LC/DC	Loading Type	Failure Criterion	N	Max Stress	Te	TC	SCFm	SCFb	SCF	R	SS Range	E/1000000	SE Range	SE TC	r	I(r)^(1/m)	ESE Range	Srange
SLM	Milled on both upper and lower surfaces	AlSi10Mg	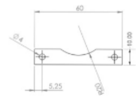	LC	Bending	Initiation	30785.28	200.572627	3	0.783381	0.5719	0.5287	1.1006	0.1	198.6752	68550	0.002898	0.0037	0.480374	1.241326	0.00298	180.5154
							39258.2	193.176056	3	0.783381	0.5719	0.5287	1.1006	0.1	191.3486	68550	0.002791	0.003563	0.480374	1.241326	0.002871	173.8585
							42059.81	177.515783	3	0.783381	0.5719	0.5287	1.1006	0.1	175.8365	68550	0.002565	0.003274	0.480374	1.241326	0.002638	159.7642
							60243.13	177.515783	3	0.783381	0.5719	0.5287	1.1006	0.1	175.8365	68550	0.002565	0.003274	0.480374	1.241326	0.002638	159.7642
							56825.58	166.739961	3	0.783381	0.5719	0.5287	1.1006	0.1	165.1626	68550	0.002409	0.003076	0.480374	1.241326	0.002478	150.066
							69195.08	164.664599	3	0.783381	0.5719	0.5287	1.1006	0.1	163.1069	68550	0.002379	0.003037	0.480374	1.241326	0.002447	148.1981
							90294.43	155.153947	3	0.783381	0.5719	0.5287	1.1006	0.1	153.6862	68550	0.002242	0.002862	0.480374	1.241326	0.002306	139.6386
							109959.2	155.153947	3	0.783381	0.5719	0.5287	1.1006	0.1	153.6862	68550	0.002242	0.002862	0.480374	1.241326	0.002306	139.6386
							96746.9	144.372993	3	0.783381	0.5719	0.5287	1.1006	0.1	143.0072	68550	0.002086	0.002663	0.480374	1.241326	0.002145	129.9357
							176751.2	143.471696	3	0.783381	0.5719	0.5287	1.1006	0.1	142.1145	68550	0.002073	0.002646	0.480374	1.241326	0.002132	129.1245
							287446.1	133.921168	3	0.783381	0.5719	0.5287	1.1006	0.1	132.6543	68550	0.001935	0.00247	0.480374	1.241326	0.00199	120.5291
							425821.2	115.232707	3	0.783381	0.5719	0.5287	1.1006	0.1	114.1426	68550	0.001665	0.002126	0.480374	1.241326	0.001712	103.7094
							646637	123.83763	3	0.783381	0.5719	0.5287	1.1006	0.1	122.6661	68550	0.001789	0.002284	0.480374	1.241326	0.00184	111.4539
							1898280	108.237683	3	0.783381	0.5719	0.5287	1.1006	0.1	107.2138	68550	0.001564	0.001997	0.480374	1.241326	0.001608	97.41392

20 **Meng Zhang 2017 0.7Po** https://www.sciencedirect.com/science/article/pii/S0921509317309772

AM Process	Post AM Treatment	Material Type	Specimen Geometry	LC/DC	Loading Type	Failure Criterion	N	Max Stress	Te	TC	SCFm	SCFb	SCF	R	SS Range	E/1000000	SE Range	SE TC	r	I(r)^(1/m)	ESE Range	Srange
L-PBF	Specimen machined by EDM, manually grinded	SS316L	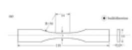	LC	Tension	Separation	38586	657.242595	3.5	0.757	1	0	1	0.1	591.5183	193000	0.003065	0.004049	0	1.2223	0.003312	591.5183
							46995	657.266458	3.5	0.757	1	0	1	0.1	591.5398	193000	0.003065	0.004049	0	1.2223	0.003312	591.5398
							100000	589.910814	3.5	0.757	1	0	1	0.1	530.9197	193000	0.002751	0.003634	0	1.2223	0.002973	530.9197
							102638.1	584.897243	3.5	0.757	1	0	1	0.1	526.4075	193000	0.002728	0.003603	0	1.2223	0.002948	526.4075
							189612.7	511.39294	3.5	0.757	1	0	1	0.1	460.2536	193000	0.002385	0.00315	0	1.2223	0.002577	460.2536
							247847.3	510.867944	3.5	0.757	1	0	1	0.1	459.7811	193000	0.002382	0.003147	0	1.2223	0.002575	459.7811
							549418.2	439.057944	3.5	0.757	1	0	1	0.1	395.1521	193000	0.002047	0.002705	0	1.2223	0.002213	395.1521
							580945.9	439.064698	3.5	0.757	1	0	1	0.1	395.1582	193000	0.002047	0.002705	0	1.2223	0.002213	395.1582
							632837.8	438.51764	3.5	0.757	1	0	1	0.1	394.6659	193000	0.002045	0.002701	0	1.2223	0.00221	394.6659

21 **Meng Zhang 2017 Po** https://www.sciencedirect.com/science/article/pii/S0921509317309772

AM Process	Post AM Treatment	Material Type	Specimen Geometry	LC/DC	Loading Type	Failure Criterion	N	Max Stress	Te	TC	SCFm	SCFb	SCF	R	SS Range	E/1000000	SE Range	SE TC	r	I(r)^(1/m)	ESE Range	Srange
L-PBF	Specimen machined by EDM, manually grinded	SS316L	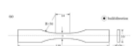	LC	Tension	Separation	36356.46	657.235391	3.5	0.757	1	0	1	0.1	591.5119	193000	0.003065	0.004049	0	1.2223	0.003312	591.5119
							55973.26	657.28762	3.5	0.757	1	0	1	0.1	591.5589	193000	0.003065	0.004049	0	1.2223	0.003313	591.5589
							84901.94	588.218762	3.5	0.757	1	0	1	0.1	529.3969	193000	0.002743	0.003623	0	1.2223	0.002964	529.3969
							116475.8	584.355138	3.5	0.757	1	0	1	0.1	525.9196	193000	0.002725	0.0036	0	1.2223	0.002945	525.9196
							214377.6	511.407798	3.5	0.757	1	0	1	0.1	460.267	193000	0.002385	0.00315	0	1.2223	0.002577	460.267
							216783.3	506.392426	3.5	0.757	1	0	1	0.1	455.7532	193000	0.002361	0.003119	0	1.2223	0.002552	455.7532
							354220	444.021537	3.5	0.757	1	0	1	0.1	399.6194	193000	0.002071	0.002735	0	1.2223	0.002238	399.6194
							409522.6	434.563065	3.5	0.757	1	0	1	0.1	391.1068	193000	0.002026	0.002677	0	1.2223	0.00219	391.1068
							398996.7	444.593358	3.5	0.757	1	0	1	0.1	400.134	193000	0.002073	0.002739	0	1.2223	0.002241	400.134

22 **Meng Zhang 2017 1.3Po** https://www.sciencedirect.com/science/article/pii/S0921509317309772

AM Process	Post AM Treatment	Material Type	Specimen Geometry	LC/DC	Loading Type	Failure Criterion	N	Max Stress	Te	TC	SCFm	SCFb	SCF	R	SS Range	E/1000000	SE Range	SE TC	r	I(r)^(1/m)	ESE Range	Srange
L-PBF	Specimen machined by EDM, manually grinded	SS316L	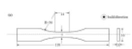	LC	Tension	Separation	42189.26	657.253401	3.5	0.757	1	0	1	0.1	591.5281	193000	0.003065	0.004049	0	1.2223	0.003312	591.5281
							54130.37	657.283568	3.5	0.757	1	0	1	0.1	591.5552	193000	0.003065	0.004049	0	1.2223	0.003313	591.5552
							99628.71	580.434332	3.5	0.757	1	0	1	0.1	522.3909	193000	0.002707	0.003576	0	1.2223	0.002925	522.3909
							179322.5	511.386186	3.5	0.757	1	0	1	0.1	460.2476	193000	0.002385	0.00315	0	1.2223	0.002577	460.2476
							312137.3	511.453274	3.5	0.757	1	0	1	0.1	460.3079	193000	0.002385	0.003151	0	1.2223	0.002578	460.3079
							400483.7	442.364154	3.5	0.757	1	0	1	0.1	398.1277	193000	0.002063	0.002725	0	1.2223	0.002229	398.1277
							417210.7	438.467212	3.5	0.757	1	0	1	0.1	394.6205	193000	0.002045	0.002701	0	1.2223	0.00221	394.6205
							521538	373.276836	3.5	0.757	1	0	1	0.1	335.9492	193000	0.001741	0.002299	0	1.2223	0.001881	335.9492
							864958.3	402.323577	3.5	0.757	1	0	1	0.1	362.0912	193000	0.001876	0.002478	0	1.2223	0.002028	362.0912
							881196.4	387.275661	3.5	0.757	1	0	1	0.1	348.5481	193000	0.001806	0.002386	0	1.2223	0.001952	348.5481
							996287.1	380.601556	3.5	0.757	1	0	1	0.1	342.5414	193000	0.001775	0.002345	0	1.2223	0.001918	342.5414

23 **Meng Zhang 2017 1.5Po** https://www.sciencedirect.com/science/article/pii/S0921509317309772

AM Process	Post AM Treatment	Material Type	Specimen Geometry	LC/DC	Loading Type	Failure Criterion	N	Max Stress	Te	TC	SCFm	SCFb	SCF	R	SS Range	E/1000000	SE Range	SE TC	r	I(r)^(1/m)	ESE Range	Srange
L-PBF	Specimen machined by EDM, manually grinded	SS316L	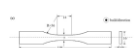	LC	Tension	Separation	22499.92	657.177308	3.5	0.757	1	0	1	0.1	591.4596	193000	0.003065	0.004048	0	1.2223	0.003312	591.4596
							27814.1	657.202972	3.5	0.757	1	0	1	0.1	591.4827	193000	0.003065	0.004048	0	1.2223	0.003312	591.4827
							35159.44	657.231338	3.5	0.757	1	0	1	0.1	591.5082	193000	0.003065	0.004049	0	1.2223	0.003312	591.5082
							71549.1	584.296155	3.5	0.757	1	0	1	0.1	525.8665	193000	0.002725	0.003599	0	1.2223	0.002945	525.8665
							84901.94	584.316867	3.5	0.757	1	0	1	0.1	525.8852	193000	0.002725	0.003599	0	1.2223	0.002945	525.8852
							160387.2	511.372678	3.5	0.757	1	0	1	0.1	460.2354	193000	0.002385	0.00315	0	1.2223	0.002577	460.2354
							162187	504.685066	3.5	0.757	1	0	1	0.1	454.2166	193000	0.002353	0.003109	0	1.2223	0.002544	454.2166
							282310.5	438.419935	3.5	0.757	1	0	1	0.1	394.5779	193000	0.002044	0.002701	0	1.2223	0.00221	394.5779
							359529.9	438.449202	3.5	0.757	1	0	1	0.1	394.6043	193000	0.002045	0.002701	0	1.2223	0.00221	394.6043
							459577.4	402.247034	3.5	0.757	1	0	1	0.1	362.0223	193000	0.001876	0.002478	0	1.2223	0.002027	362.0223
							702306.4	365.509065	3.5	0.757	1	0	1	0.1	328.9582	193000	0.001704	0.002252	0	1.2223	0.001842	328.9582
							985230.8	364.992625	3.5	0.757	1	0	1	0.1	328.4934	193000	0.001702	0.002248	0	1.2223	0.001839	328.4934

24 **EPRI Report (room temperature)**

AM Process	Post AM Treatment	Material Type	Specimen Geometry	LC/DC	Loading Type	Failure Criterion	N	Δε	Te	TC	SCF	SCFb	SCF	Max S	SS Range	E/1000000	SE Range	SE TC	r	I(r)^(1/m	ESE Rang	Srange
L-PBF	Annealed HIP	SS316L	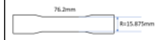	DC	Tension	Separation	2202	0.016	7.9375	0.631059	1	0	1	1560	3120	195000	0.016	0.025354	0	1.5426	0.016436	3120
							2821	0.016	7.9375	0.631059	1	0	1	1560	3120	195000	0.016	0.025354	0	1.5426	0.016436	3120
							5160	0.012	7.9375	0.631059	1	0	1	1170	2340	195000	0.012	0.019016	0	1.5426	0.012327	2340
							4693	0.012	7.9375	0.631059	1	0	1	1170	2340	195000	0.012	0.019016	0	1.5426	0.012327	2340
							6229	0.008	7.9375	0.631059	1	0	1	780	1560	195000	0.008	0.012677	0	1.5426	0.008218	1560
							13227	0.008	7.9375	0.631059	1	0	1	780	1560	195000	0.008	0.012677	0	1.5426	0.008218	1560
							254532	0.004	7.9375	0.631059	1	0	1	390	780	195000	0.004	0.006339	0	1.5426	0.004109	780
							86286	0.004	7.9375	0.631059	1	0	1	390	780	195000	0.004	0.006339	0	1.5426	0.004109	780
							51370	0.00514	7.9375	0.631059	1	0	1	501.15	1002.3	195000	0.00514	0.008145	0	1.5426	0.00528	1002.3
							53154	0.00513	7.9375	0.631059	1	0	1	500.175	1000.35	195000	0.00513	0.008129	0	1.5426	0.00527	1000.35

25 **EPRI Report (300C)**

AM Process	Post AM Treatment	Material Type	Specimen Geometry	LC/DC	Loading Type	Failure Criterion	N	Δε	Te	TC	SCF	SCFb	SCF	Max S	SS Range	E/1000000	SE Range	SE TC	r	I(r)^(1/m	ESE Rang	Srange
L-PBF	Annealed HIP	SS316L		DC	Tension	Separation	26420	0.006	7.9375	0.631059	1	0	1	585	1170	195000	0.006	0.009508	0	1.5426	0.006164	1170
							25536	0.0061	7.9375	0.631059	1	0	1	594.75	1189.5	195000	0.0061	0.009666	0	1.5426	0.006266	1189.5
							7000	0.012	7.9375	0.631059	1	0	1	1170	2340	195000	0.012	0.019016	0	1.5426	0.012327	2340
							7000	0.012	7.9375	0.631059	1	0	1	1170	2340	195000	0.012	0.019016	0	1.5426	0.012327	2340

26 **Rakish Shrestha 2021 Axial, AB, Machine A** https://www.sciencedirect.com/science/article/pii/S0142112320305958

AM Process	Post AM Treatment	Material Type	Specimen Geometry	LC/DC	Loading Type	Failure Criterion	N	Max Stress	Te	TC	SCFm	SCFb	SCF	R	SS Range	E/1000000	SE Range	SE TC	r	I(r)^(1/m	ESE Rang	Srange
LB-PBF	Annealed	SS316L	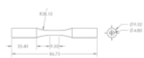	LC	Tension	Separation	268515	250	2.4	0.823206	1	0	1	-1	500	193000	0.00332	0.004033	0	1.2223	0.0033	500
							392660	250	2.4	0.823206	1	0	1	-1	500	193000	0.00332	0.004033	0	1.2223	0.0033	500
							70737	300	2.4	0.823206	1	0	1	-1	600	193000	0.00426	0.005175	0	1.2223	0.004234	600
							83110	300	2.4	0.823206	1	0	1	-1	600	193000	0.00426	0.005175	0	1.2223	0.004234	600
							18909	325	2.4	0.823206	1	0	1	-1	650	193000	0.00516	0.006268	0	1.2223	0.005128	650
							22195	325	2.4	0.823206	1	0	1	-1	650	193000	0.00516	0.006268	0	1.2223	0.005128	650
							3428	350	2.4	0.823206	1	0	1	-1	700	193000	0.006	0.007289	0	1.2223	0.005963	700
							5325	350	2.4	0.823206	1	0	1	-1	700	193000	0.006	0.007289	0	1.2223	0.005963	700

27 **Rakish Shrestha 2021 R-B, AB, Machine A** https://www.sciencedirect.com/science/article/pii/S0142112320305958

AM Process	Post AM Treatment	Material Type	Specimen Geometry	LC/DC	Loading Type	Failure Criterion	N	Max Stress	Te	TC	SCFm	SCFb	SCF	R	SS Range	E/1000000	SE Range	SE TC	r	I(r)^(1/m	ESE Rang	Srange
LB-PBF	Annealed	SS316L		LC	Bending	Separation	374100	250	2.38	0.824738	0.393629	0.681128	1.074757	-1	537.3785	193000	0.003568	0.004326	0.633751	1.256103	0.003444	500
							852400	250	2.38	0.824738	0.393629	0.681128	1.074757	-1	537.3785	193000	0.003568	0.004326	0.633751	1.256103	0.003444	500
							203800	300	2.38	0.824738	0.393629	0.681128	1.074757	-1	644.8542	193000	0.004578	0.005551	0.633751	1.256103	0.00442	600
							125400	325	2.38	0.824738	0.393629	0.681128	1.074757	-1	698.5921	193000	0.005546	0.006724	0.633751	1.256103	0.005353	650
							96800	325	2.38	0.824738	0.393629	0.681128	1.074757	-1	698.5921	193000	0.005546	0.006724	0.633751	1.256103	0.005353	650
							69500	350	2.38	0.824738	0.393629	0.681128	1.074757	-1	752.3299	193000	0.006449	0.007819	0.633751	1.256103	0.006225	700
							103700	350	2.38	0.824738	0.393629	0.681128	1.074757	-1	752.3299	193000	0.006449	0.007819	0.633751	1.256103	0.006225	700

28 **Rakish Shrestha 2019 Machined H** https://www-sciencedirect-com.proxy.lib.umich.edu/science/article/pii/S2214860419300065

AM Process	Post AM Treatment	Material Type	Specimen Geometry	LC/DC	Loading Type	Failure Criterion	N	Δε	Te	TC	SCF	SCFb	SCF	Max S	SS Range	E/1000000	SE Range	SE TC	r	I(r)^(1/m	ESE Rang	Srange
LB-PBF	Machined using lathe, polished with sand paper	SS316L	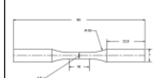	DC	Tension	Separation	627274	0.002	1.725	0.885891	1	0	1	193	386	193000	0.002	0.002258	0	1.5426	0.001464	386
							324363	0.002	1.725	0.885891	1	0	1	193	386	193000	0.002	0.002258	0	1.5426	0.001464	386
							141491	0.003	1.725	0.885891	1	0	1	289.5	579	193000	0.003	0.003386	0	1.5426	0.002195	579
							130161	0.003	1.725	0.885891	1	0	1	289.5	579	193000	0.003	0.003386	0	1.5426	0.002195	579
							28571	0.004	1.725	0.885891	1	0	1	386	772	193000	0.004	0.004515	0	1.5426	0.002927	772
							21327	0.004	1.725	0.885891	1	0	1	386	772	193000	0.004	0.004515	0	1.5426	0.002927	772
							7416	0.006	1.725	0.885891	1	0	1	579	1158	193000	0.006	0.006773	0	1.5426	0.004391	1158
							6541	0.006	1.725	0.885891	1	0	1	579	1158	193000	0.006	0.006773	0	1.5426	0.004391	1158
							1838	0.008	1.725	0.885891	1	0	1	772	1544	193000	0.008	0.00903	0	1.5426	0.005854	1544
							1271	0.008	1.725	0.885891	1	0	1	772	1544	193000	0.008	0.00903	0	1.5426	0.005854	1544

29 **Rakish Shrestha 2019 Machined V** https://www-sciencedirect-com.proxy.lib.umich.edu/science/article/pii/S2214860419300065

AM Process	Post AM Treatment	Material Type	Specimen Geometry	LC/DC	Loading Type	Failure Criterion	N	Δε	Te	TC	SCF	SCFb	SCF	Max S	SS Range	E/1000000	SE Range	SE TC	r	I(r)^(1/m	ESE Rang	Srange
LB-PBF	Machined using lathe, polished with sand paper	SS316L	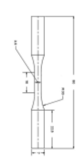	DC	Tension	Separation	476241	0.002	1.725	0.885891	1	0	1	193	386	193000	0.002	0.002258	0	1.5426	0.001464	386
							414272	0.002	1.725	0.885891	1	0	1	193	386	193000	0.002	0.002258	0	1.5426	0.001464	386
							98876	0.003	1.725	0.885891	1	0	1	289.5	579	193000	0.003	0.003386	0	1.5426	0.002195	579
							52254	0.003	1.725	0.885891	1	0	1	289.5	579	193000	0.003	0.003386	0	1.5426	0.002195	579
							22644	0.004	1.725	0.885891	1	0	1	386	772	193000	0.004	0.004515	0	1.5426	0.002927	772
							15479	0.004	1.725	0.885891	1	0	1	386	772	193000	0.004	0.004515	0	1.5426	0.002927	772
							2113	0.006	1.725	0.885891	1	0	1	579	1158	193000	0.006	0.006773	0	1.5426	0.004391	1158
							1944	0.006	1.725	0.885891	1	0	1	579	1158	193000	0.006	0.006773	0	1.5426	0.004391	1158
							2175	0.008	1.725	0.885891	1	0	1	772	1544	193000	0.008	0.00903	0	1.5426	0.005854	1544
							1778	0.008	1.725	0.885891	1	0	1	772	1544	193000	0.008	0.00903	0	1.5426	0.005854	1544

30	Rakish Shrestha 2019 Machined D https://www-sciencedirect-com.proxy.lib.umich.edu/science/article/pii/S2214860419300065																						
	AM Process	Post AM Treatment	Material Type	Specimen Geometry	LC/DC	Loading Type	Failure Criterion	N	Δε	Te	TC	SCF	SCFb	SCF	Max S	SS Range	E/100000(	SE Range	SE TC	r	I(r)^(1/m	ESE Rang	Srange
	LB-PBF	Machined using lathe, polished with sand paper	SS316L	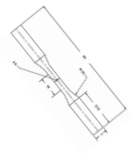	DC	Tension	Separation	168700	0.002	1.725	0.885891	1	0	1	193	386	193000	0.002	0.002258	0	1.5426	0.001464	386
								146531	0.002	1.725	0.885891	1	0	1	193	386	193000	0.002	0.002258	0	1.5426	0.001464	386
								44936	0.003	1.725	0.885891	1	0	1	289.5	579	193000	0.003	0.003386	0	1.5426	0.002195	579
								29938	0.003	1.725	0.885891	1	0	1	289.5	579	193000	0.003	0.003386	0	1.5426	0.002195	579
								14940	0.004	1.725	0.885891	1	0	1	386	772	193000	0.004	0.004515	0	1.5426	0.002927	772
								3641	0.004	1.725	0.885891	1	0	1	386	772	193000	0.004	0.004515	0	1.5426	0.002927	772
								1046	0.006	1.725	0.885891	1	0	1	579	1158	193000	0.006	0.006773	0	1.5426	0.004391	1158
								942	0.006	1.725	0.885891	1	0	1	579	1158	193000	0.006	0.006773	0	1.5426	0.004391	1158
								2206	0.008	1.725	0.885891	1	0	1	772	1544	193000	0.008	0.00903	0	1.5426	0.005854	1544
								1112	0.008	1.725	0.885891	1	0	1	772	1544	193000	0.008	0.00903	0	1.5426	0.005854	1544

31	Rakish Shrestha 2019 As-built V https://www-sciencedirect-com.proxy.lib.umich.edu/science/article/pii/S2214860419300065																						
	AM Process	Post AM Treatment	Material Type	Specimen Geometry	LC/DC	Loading Type	Failure Criterion	N	Δε	Te	TC	SCF	SCFb	SCF	Max S	SS Range	E/100000(	SE Range	SE TC	r	I(r)^(1/m	ESE Rang	Srange
	LB-PBF		SS316L	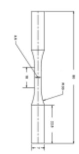	DC	Tension	Separation	156101	0.002	1.725	0.885891	1	0	1	193	386	193000	0.002	0.002258	0	1.5426	0.001464	386
								154239	0.002	1.725	0.885891	1	0	1	193	386	193000	0.002	0.002258	0	1.5426	0.001464	386
								59460	0.003	1.725	0.885891	1	0	1	289.5	579	193000	0.003	0.003386	0	1.5426	0.002195	579
								55891	0.003	1.725	0.885891	1	0	1	289.5	579	193000	0.003	0.003386	0	1.5426	0.002195	579
								15540	0.004	1.725	0.885891	1	0	1	386	772	193000	0.004	0.004515	0	1.5426	0.002927	772
								11496	0.004	1.725	0.885891	1	0	1	386	772	193000	0.004	0.004515	0	1.5426	0.002927	772
								7593	0.006	1.725	0.885891	1	0	1	579	1158	193000	0.006	0.006773	0	1.5426	0.004391	1158
								7152	0.006	1.725	0.885891	1	0	1	579	1158	193000	0.006	0.006773	0	1.5426	0.004391	1158
								3200	0.008	1.725	0.885891	1	0	1	772	1544	193000	0.008	0.00903	0	1.5426	0.005854	1544
								2137	0.008	1.725	0.885891	1	0	1	772	1544	193000	0.008	0.00903	0	1.5426	0.005854	1544

32	Rakish Shrestha 2019 As-built D https://www-sciencedirect-com.proxy.lib.umich.edu/science/article/pii/S2214860419300065																						
	AM Process	Post AM Treatment	Material Type	Specimen Geometry	LC/DC	Loading Type	Failure Criterion	N	Δε	Te	TC	SCF	SCFb	SCF	Max S	SS Range	E/100000(	SE Range	SE TC	r	I(r)^(1/m	ESE Rang	Srange
	LB-PBF		SS316L	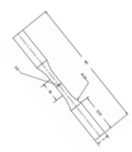	DC	Tension	Separation	115240	0.002	1.725	0.885891	1	0	1	193	386	193000	0.002	0.002258	0	1.5426	0.001464	386
								104694	0.002	1.725	0.885891	1	0	1	193	386	193000	0.002	0.002258	0	1.5426	0.001464	386
								33065	0.003	1.725	0.885891	1	0	1	289.5	579	193000	0.003	0.003386	0	1.5426	0.002195	579
								24474	0.003	1.725	0.885891	1	0	1	289.5	579	193000	0.003	0.003386	0	1.5426	0.002195	579
								14126	0.004	1.725	0.885891	1	0	1	386	772	193000	0.004	0.004515	0	1.5426	0.002927	772
								11816	0.004	1.725	0.885891	1	0	1	386	772	193000	0.004	0.004515	0	1.5426	0.002927	772
								2972	0.006	1.725	0.885891	1	0	1	579	1158	193000	0.006	0.006773	0	1.5426	0.004391	1158
								2494	0.006	1.725	0.885891	1	0	1	579	1158	193000	0.006	0.006773	0	1.5426	0.004391	1158
								1667	0.008	1.725	0.885891	1	0	1	772	1544	193000	0.008	0.00903	0	1.5426	0.005854	1544
								1547	0.008	1.725	0.885891	1	0	1	772	1544	193000	0.008	0.00903	0	1.5426	0.005854	1544

APPENDIX B: FATIGUE TEST SPECIMEN DRAWINGS

AM Fatigue Specimen - DEN

All dimensions are in mm.
Tolerance = +/- 0.025 mm.
Surface roughness = As per industrial best practices.

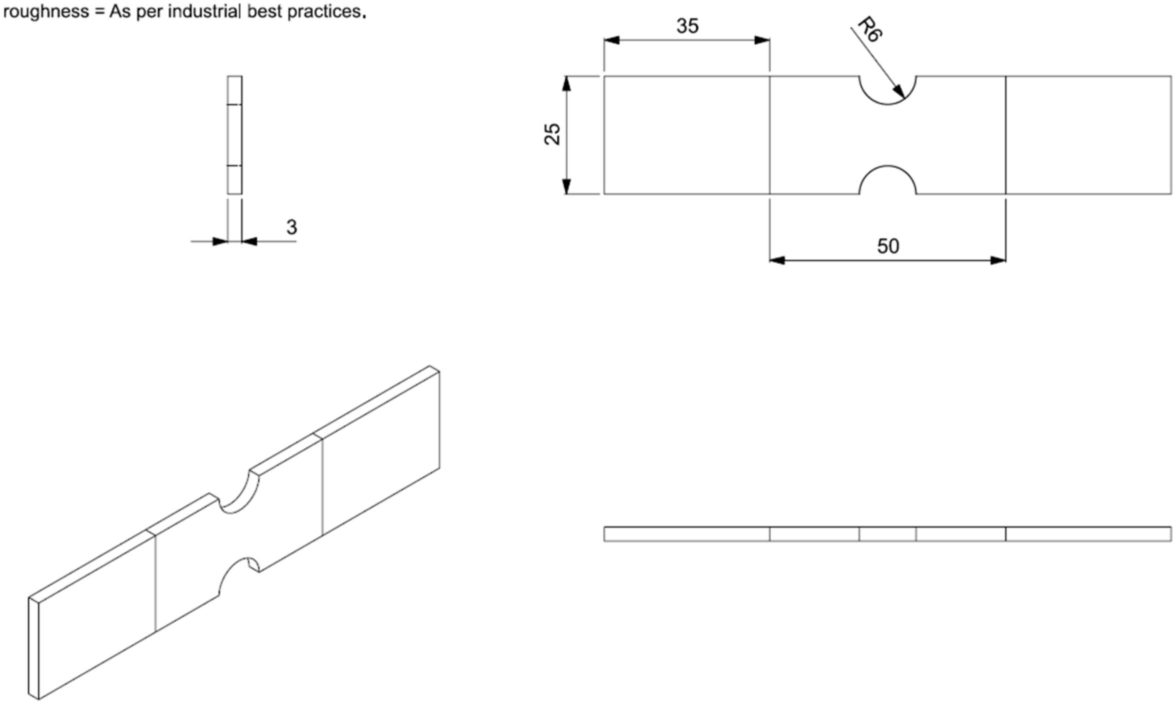

AM Fatigue Specimen - DEN

All dimensions are in mm.
Tolerance = +/- 0.025 mm.
Surface roughness = As per industrial best practices.